

STATEMENT

Name: **Kristóf Furuglyás**

Neptun ID: AHMITR

ELTE Faculty of Science: Physics MSc

specialization: Scientific Data Analytics and Modeling

Title of diploma work: Analysis of the Functional Connectivity of the Brain During Multimodal Signal Processing

As the author of the diploma work I declare, with disciplinary responsibility that my thesis is my own intellectual product and the result of my own work. Furthermore I declare that I have consistently applied the standard rules of references and citations.

I acknowledge that the following cases are considered plagiarism:

- using a literal quotation without quotation mark and adding citation;
- referencing content without citing the source;
- representing another person's published thoughts as my own thoughts.

Furthermore, I declare that the printed and electronical versions of the submitted diploma work are textually and contextually identical.

Budapest, 28 May 2020.



Signature of Student

EÖTVÖS LORÁND UNIVERSITY
FACULTY OF SCIENCE

**ANALYSIS OF THE FUNCTIONAL
CONNECTIVITY OF THE BRAIN
DURING MULTIMODAL SIGNAL
PROCESSING**

KRISTÓF FURUGLYÁS

Thesis, Physics MSc.

Consultant:

Zoltán Somogyvári, Ph.D.

Dept. of Computational Sciences, Wigner Research Centre for Physics

Internal advisor:

Imre Derényi, Ph.D.

Dept. of Biological Physics, Eötvös Loránd University

2020



Budapest, Hungary, 2020

Acknowledgements

I would like to thank my supervisor, Zoltán Somogyvári Ph. D., for guidance through the years, for professional pieces of advice and for constant motivation.

I would like to acknowledge László Négyessy Ph. D. for helping understanding biological phenomena and Zsigmond Benkő, a fellow colleague, who gave suggestions on data analysis.

I would like to thank all the other members of our research group from Wigner RCP for their remarks on this thesis.

I would also like to thank Umberto Olcese and his research group for conducting the experiments.

My girlfriend kept me sane and motivated during difficult times under lockdown and quarantine. For this, I am very grateful.

Abstract

Mismatch negativity (MMN) is a component of the event-related potential (ERP) to an odd stimulus in a sequence of stimuli. It has been found in different forms, in different regions of the brain. The common point in all is that they include a so-called surprise enhancement or the genuine mismatch, due to learning by error. The repetition suppression is a reduction of neural response which is also present in the feedback.

In our work, we analysed the response of the brain areas whilst the animal had been presented bimodal (auditory and visual) stimulus. My main objective was to create such analysing equipment that can help our understanding about the data and to draw preliminary biological conclusions about the main features of the results – in the aspect of signal processing. These results should be brief, concise and straightforward while keeping the maximum amount of information.

These methods were the following: simple point-by-point statistical testing between the temporal signals, analysis of the activity of the previously identified neural cells, hypothesis testing on the difference of the frequency spectra and measuring the spatial coherence inside and between the primary visual and anterolateral cortices. All of them showed the effect of fatigue and the non-novel mismatches such as visual, auditory and bimodal. We also noticed the emergence of a possible conditional mismatch negativity, which denotes the dependence between the sensory inputs. Stimulus specific adaptation was also present and the effect of varied inter-stimulus interval on the neurons excitatory state, too.

These methods are ready to be tested on multiple animals and our theories will either be confirmed or disproved. On a larger scale, these are only dependent on the animal in terms of frequency bands, therefore are easily applicable for others also.

Contents

1	Introduction	1
1.1	Goals	1
1.2	From brain to neuron	1
1.3	Monitoring brain activity	4
1.4	Mismatch negativity	5
1.5	General characteristics of the MMN	7
1.5.1	MMN underlying mechanisms	8
1.6	Stimulus-specific adaptation and deviance detection	10
2	Experiment	12
3	Data processing and evaluation methods	16
3.1	Temporal evaluation	16
3.2	Spiking histograms	16
3.3	Frequency map	17
3.3.1	Frequency conversion	17
3.3.2	Creating map	18
3.4	Coherence of cortical areas in frequency bands	18
4	Results	20
4.1	Temporal evaluation	20
4.2	Spiking histograms	26
4.2.1	Dominant cells	28
4.3	Frequency map	32
4.3.1	Average Fourier spectra	33
4.3.2	Creating frequency map	36
4.3.3	Visual MMN	37
4.3.4	Auditory MMN	39
4.3.5	Bimodal MMN	40
4.3.6	Non-mismatch comparisons	42
4.4	Coherence of cortical areas in frequency bands	43
4.4.1	Mismatch comparisons	45
4.4.2	Non-mismatch comparisons	47
5	Discussion	51
6	References	52
	Appendices	59

A	Temporal evaluation	59
A.1	Primary visual cortex (V1)	59
A.2	Anterolateral cortex (AL)	62
B	Spiking histograms	66
C	Frequency map	68

1 Introduction

The perception and signal processing of the brain have been under constant research for decades. Many aspects have been explored, yet, more are to be discovered. Analyses of the neural responses under outer stimulation helped us to get a deeper knowledge about signal processing but only few of them consisted the connection of multiple sensory inputs.

The novelty our experiment carries within itself is the effect of bimodal stimulation of the brain. Mice were presented an auditory and visual stimuli at the same time under different paradigms. Paradigms consisted of full mismatch detection task (traditional oddball sequences), equiprobable series and an only standard session, where the inter-stimulus interval (ISI) was 12 seconds instead of 1.5.

This thesis concentrates on the evaluation and analysing process in signal processing terms. Many more tools and sets of parameters could have been useful, too, but these were the one which found the same effects for this particular animal. To draw biological conclusions it will be inevitable to run these methods on multiple animals to overcome problems which we will discuss later.

1.1 Goals

Primary objectives for this project were generating a scheme that helps us gather an overall picture of the mismatch types (auditory, visual and bimodal), the methodical differences (traditional, genuine mismatch and the role of ISI) and the cortices of the brain. We had to create a framework that is applicable for more animals, yet, capable to create a ground truth at the same time. The main challenge therefore yields itself; create brief explanatory results that provides us the most available information. To achieve this, one shall utilise multiple tools in order not to lose any message.

Throughout the document I will elaborate on simple temporal significance detection via hypothesis testing and firing rates of individual (previously identified) neuronal cells. Later, with the Fourier transform of the signals, hypothesis testing is going to done once more on the raw absolute value of the frequency spectra of channels, and finally, coherence inside and in between the brain regions are going to be calculated to reveal those effects which either affect both of the cortices or all of the brain.

1.2 From brain to neuron

The human brain is one of the most amazing organs the nature has developed with its complexity and adaptability. Made up of about 86 billion neurons and the same amount of other non-neuronal cells [1] it is believed to consume one-fifth of the body's total

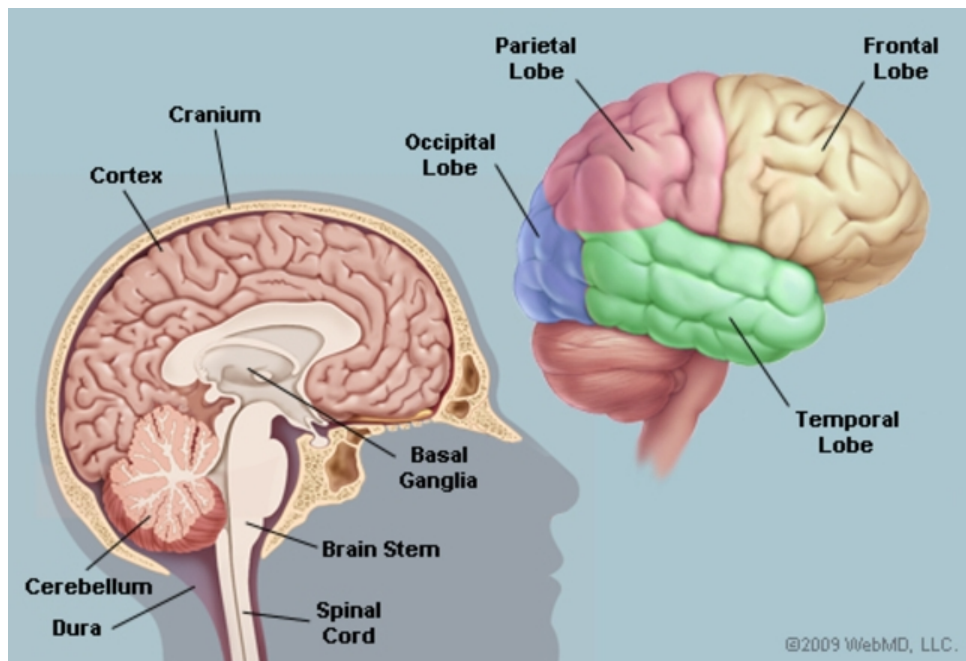
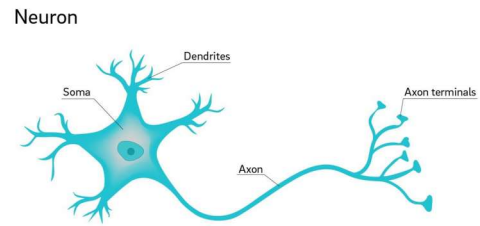
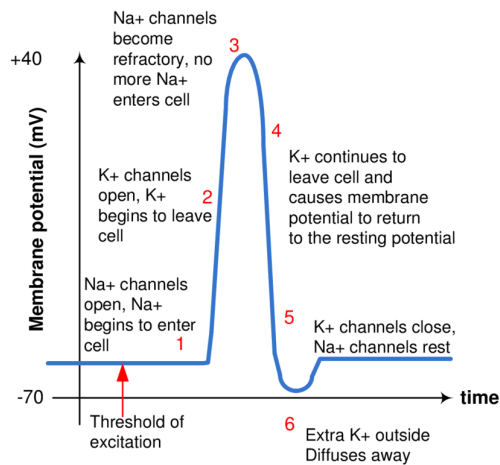


Figure 1. **Anatomy of the human brain.** On the left hand side the structure of the brain is visible, and on the right hand side the functional connectivity. Source: Matthew Hoffman, MD © 2014 WebMD, LLC

energy needs whilst awake [2]. Due its complexity, very little information is known about how it processes the input. However, animal experiments seem to resolve this mysterious organ using the similarities between a human's and other animals' brain. Since we gather information from the outer world in multiple channels, we need to dig deeper in the connection between the inputs. We are familiar with various aspects of information processing (e.g., hierarchical, predictive, etc.) but not so much with the multimodal integration of them.

The brain is part of the central nervous system and consists of the cerebrum (including the cerebral cortex and the basal ganglia), the brainstem and the cerebellum. There are four lobes within the cerebrum (frontal, temporal, parietal and occipital) in which areas are defined as they are associated with specific functions, such as the sensory, motor and association regions (fig. 1.). Even though the two hemispheres of the brain are more-or-less similar in structure and function, there are functions which are associated with only one side, e.g., language in the left and visual-spatial ability in the right. Underneath the cerebral cortex there are numerous systems such as the thalamus, the hypothalamus or the amygdala.

The basic computational unit of the brain is the neuron. These nerve cells have the capability of being electrically excitable [3] and communicating with each other via specialised connections called synapses. A typical neuron consists of three parts which are the soma (cell body), dendrites and one axon. The soma is the core element creating a



(a) **An approximate plot of a typical action potential with its 6 phases** The electrical membrane potential is seen in the aspect of time which takes about 3-5 milliseconds. Source: [4].

(b) **Illustration of a neuron.** Credit: David Baillot / UC San Diego

Figure 2. **Figures about a neuron.**

bridge between its filaments, the axon and the dendrites. The soma is the key element by thresholding the inputs and calculating its outputs. Dendrites typically branch towards other cells and extend a few hundred micrometers from the soma. The axon is the output compartment carrying the stimulus and can reach up to centimetres. We can divide the neurons based on their activity into two groups: excitatory and inhibitory. Excitatory cells can be principal cells whose axons leave their original area and connect to others (pyramidal cells of the 5th layer). Inhibitor neurons are interneurons and typically do not leave their neighbourhoods. However, there are exceptions; the Purkinje cells do leave the cerebellum and spiny stellate cells stay in the sensory cortex. The main neurotransmitters are the glutamate for excitatory and GABA for inhibitory cells.

Signalling process is elicited by a change in the electro-chemical potentials. Neurons are electrically excitable, due to maintenance of voltage gradients across their membranes. Chemical processes are mediated through ion-channels, mainly potassium, sodium and chlorine channels. A quick and sufficiently powerful change in the potential causes the neuron to generate an all-or-nothing electrochemical pulse termed action potential (fig. 2a.). Once it reaches a synapse through the axon, the signal is then passed on to the dendrite of an other cell. Action potentials in neurons are also known as *nerve impulses* or *spikes*, and the temporal sequence of action potentials generated by a neuron is called its *spike train*. A neuron that emits an action potential, or nerve impulse, is often said to *fire*.

Multiple neurons communicating with each other forms a neural circuit. Due to the additivity of electrical charge, these circuits can form a longer temporal signal. Depending

on the number of neurons and the outer circumstances, these signals can last up to seconds. The change in the local field potential (LFP) is an overall summary of the neurons (or neuron populations). Most basic characteristics of a neuron include for example summing the input voltages from its inputs then firing depending on the result of that. These tend to be in the range of millivolts.

1.3 Monitoring brain activity

With the help of electroencephalographic (EEG) devices the electric potential of the brain can be measured directly. Non-invasive EEG-s measure the potential on the scalp while the invasive ones' sensors are placed onto the cortex (electrocorticographs). To measure the LFP intracranial electrodes are often put inside the brain, which are most of the times spikes or shanks having an efficient setup to measure layer-specific phenomena. EEG is mainly used for medical purposes, however, lately it has become a tool for commercial purposes (apart from the scientific); e.g., what are the brain's responses to different advertisements or for gaming and military uses. Observing brain activity via electric potential gives us the opportunity to look deep into its functional behaviour. In the field of medical use, among many others, EEG can be a beneficial to detect sleeping disorders as well as the depth of anaesthesia during a surgery but is mainly utilised when an epileptic patient needs a surgery and drugs no longer work. Often one can create the so-called evoked potential which are time-locked to an outer stimulus; these stimuli can be visual, tactile or auditory. Event-related potentials are different from the evoked ones in such a way that there is a cognitive or motor process that is being measured. ERPs are caused directly by an outer stimulus while the evoked potentials are supposed to have the source inside the brain. These ERPs can influence the brain waves.

An event-related potential (ERP) is the measured brain response that is the direct result of a specific sensory, cognitive, or motor event. More formally, it is any stereotyped electrophysiological response to a stimulus. The study of the brain in this way provides a noninvasive means of evaluating brain functioning. Currently, ERP is one of the most widely used methods in cognitive neuroscience research to study the physiological correlates of sensory, perceptual and cognitive activity associated with processing information. The EEG reflects thousands of simultaneously ongoing brain processes. This means that the brain response to a single stimulus or event of interest is not usually visible in the EEG recording of a single trial. We can always see the brain's response but not the stimulus-specific part. To see the latter, too, the experimenter must conduct many trials and average the results together, causing random brain activity to be averaged out and the relevant waveform to remain, called the ERP. In equation 1. the averaged signal ($\bar{x}(t)$)

is the mean of N number of responses in every data point $x(t, k)$ and can be decomposed into the real underlying pure signal $s(t)$ and a sequence of uncorrelated noise $n(t, k)$ [5].

$$\bar{x}(t) = \frac{1}{N} \sum_{k=1}^N x(t, k) = s(t) + \frac{1}{N} \sum_{k=1}^N n(t, k). \quad (1)$$

ERP waveforms consist of a series of positive and negative voltage deflections, which are related to a set of underlying components. Though some ERP components are referred to with acronyms (e.g., contingent negative variation – CNV, error-related negativity – ERN), most components are referred to by a letter (N/P) indicating polarity (negative/positive), followed by a number indicating either the latency in milliseconds or the component’s ordinal position in the waveform. For instance, a negative-going peak that is the first substantial valley in the waveform and often occurs about 200 milliseconds after a stimulus is presented is often called the N200 (indicating its latency is 200 ms after the stimulus and that it is negative) or N2 (indicating that it is the first peak and is negative). N200 is primarily distributed over anterior brain regions, posterior distributions have been reported in visual attention paradigms, such as visual search [7]. It is often followed by a positive peak, usually called the P300 or P3, which is thought to reflect processes involved in stimulus evaluation or categorisation [8]. For example, on fig. 3. one can see the ERP of a mouse recorded in the primary visual cortex. However, this recording was not done with EEG, but with planted electrodes and the polarity of the signal is diverse through the literature. The stated latencies for ERP components are often quite variable, particularly so for the later components that are related to the cognitive processing of the stimulus. However, peaks of the ERP can vary depending on animal, stimulus type and location site.

It is interesting that how many functional disorders can be noticed via ERP-s. ERP component abnormalities in clinical research have been shown in neurological conditions such as: ADHD, Parkinson’s disease, multiple sclerosis, schizophrenia or obsessive-compulsive disorder. Therefore the differences from a well known signal can be the indicator of abnormalities. But many times the discrepancy is not an indicator of a medical condition but rather a somewhat surprise. The detection of violations to regularities in the sound stream may be critical for survival also. This brings us to our next point, the mismatch negativity.

1.4 Mismatch negativity

Mismatch negativity (MMN) is a negative component of the event-related response in an EEG signal, elicited by any perceptible and infrequent change in some repetitive aspect of an auditory (e.g., stimulus pitch, stimulus duration) or a visual stimulation [9]. It is the brain’s response to the violations of a rule, established by a sequence of sensory stimuli [10]. Sometimes the entire sequence is called an oddball sequence which includes

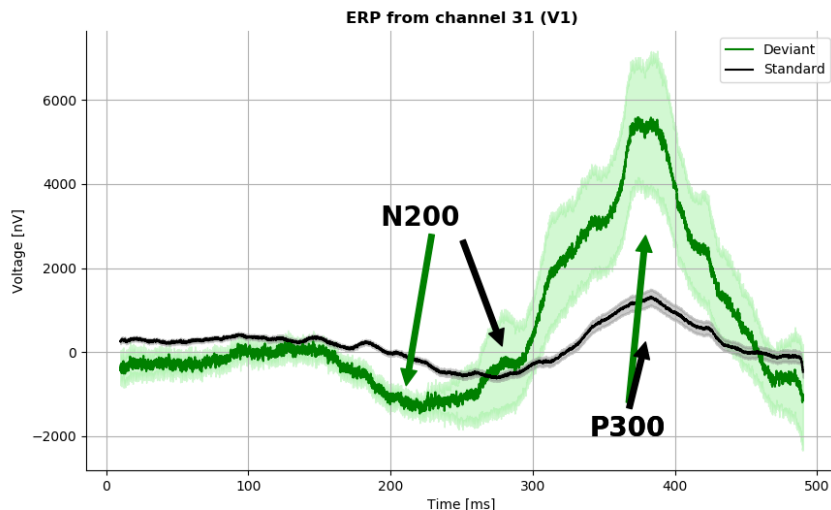


Figure 3. **ERPs of a standard and an auditory deviant signal.** Data are from our experiment for bimodal stimulation and the standard error of means are shown in the shaded areas. Channel is from the primary visual cortex (V1) and labelling of the peaks is based on [6].

the standard signals (*s*) that are being repeated continuously and a deviant one (*d*). The MMN is the difference between the standard and deviant signal.

The MMN can be elicited regardless of whether the subject is paying attention to the sequence. This reflects the brain's ability to perform automatic comparisons between consecutive stimuli and provides an electrophysiological index of sensory learning and perceptual accuracy. During auditory stimulation, a person can be reading or watching a silent subtitled movie, yet still show a clear MMN [11]. Even though MMN have been studied mainly in the auditory cortex, some studies show evidence of visual MMN (vMMN) [12, 13, 14]. A potential analogue to the MMN has also been reported in the somatosensory system which seems to be generated in fine discrimination tasks [15]. The MMN is associated with a cortical operation of comparing the sensory input with the memory trace. Given its automatic nature, the MMN might be associated with pre-attentive cognitive operations in audition and, for this reason it has been suggested that it reflects 'primitive intelligence' in the auditory cortex [16].

It is worth mentioning in a paragraph how widespread the use of MMN is. The most consistent observation including event-related potentials (ERPs) is about the reduction of amplitude of the MMN in schizophrenic patients compared with healthy control subjects. Another important application is in the field of dyslexia: dyslexic patients show diminished MMN, albeit only for frequency deviants and not for duration signalling an auditory frequency discrimination impairment [17]. Another example is shown on fig 4. The amyotrophic lateral sclerosis patients' MMN signals significantly differ in later

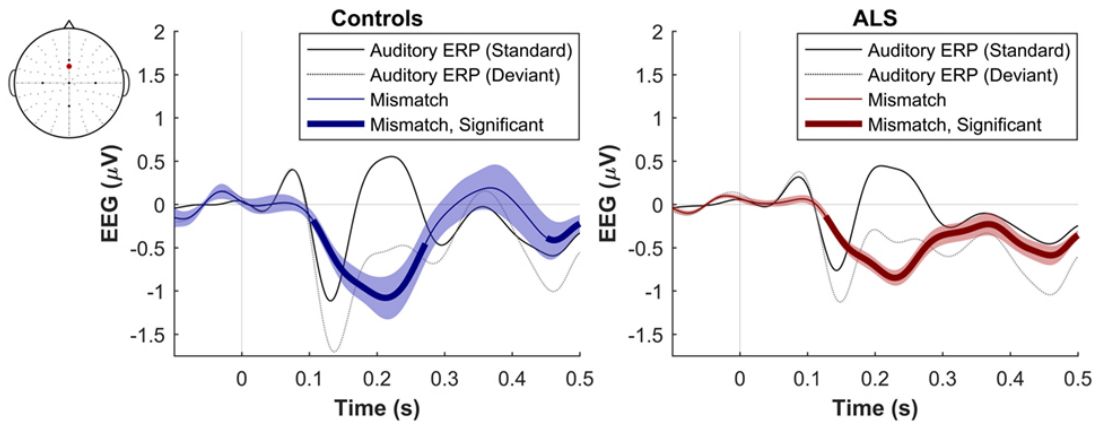


Figure 4. **Presence of robust mismatch negativity.** Responses were recorded in both ALS-patient and control groups. The auditory event-related potentials (ERPs), as well as their difference are shown. The shades indicate the standard error of the mean. Source: [18].

temporal regions [18].

1.5 General characteristics of the MMN

MMN is thought to peak at about 150-250 ms after change onset, which depends on the experimental paradigm. Difference in paradigms mean either a change in inter-stimulus interval (ISI), intensity, duration, frequency, location or lack of the stimulus. These type of changes themselves could be able to create whole new chapters for the study of MMN [24]. Multiple paradigms help researches in the clinical fields break down the original MMN into its main components. It is generally believed that any violation of the acoustic regularity pattern can induce MMN [16]. Furthermore, MMN has also been detected with spectrally rich stimuli, indicating attentive pitch discrimination in comparison to pure sinusoidal tones [25].

Memory traces could be an indicative of the processing of multiple standard stimuli and if the deviant comes while this trace is active then the automatic change detector is alarmed giving rise to a mismatch. The length of this period – also called *echoic memory* – has been reported to last at least 10 s in normal subjects [26].

MMN can be measured even the state of coma it is a predictor for the recovery of consciousness [27]. MMN is clearly shown without any task requirements or when the task is not even related to the stimulus. This potential makes it particularly suitable for testing different clinical populations [28]. On the other hand, to avoid overlap with other ERP components (other dedicated peaks and valleys such as the error-related negativity (ERN) or contingent negative variaton (CNV)), during visual MMN tasks the best condition to observe the phenomenon is when subject attention is directed away

from the stimulus [29]. During MMN there is an involuntary attention switching in particular, over the source in the frontal lobe [30].

1.5.1 MMN underlying mechanisms

Even though myriad of research have been investigating the emergence of mismatch negativity, relatively few tried to explain the underlying mechanisms that formulate those particular patterns. In this section I am going to describe the two major hypotheses that emerged: the *model adjustment* and the *adaptation* hypothesis, and later introduce a unifying framework described by Garrido et al., the *predictive coding* [23].

Model adjustment The model adjustment states that the MMN is an index of automatic change detection governed by a pre-attentive sensory memory mechanism i.e. marker for error detection [32]. It is the result from the difference between current and preceding input suggesting that a memory trace still remains from the previous stimuli [10]. MMN could reflect on-line modifications and be a signal for when the brain updates its model upon discrepancy between the input and prediction. In that sense, MMN is the result of the comparison [33, 34, 35]. An explanation was given by Giard et al. in 1990 including two factors that build up MMN; a sensory memory mechanism (related to temporal processes) and an automatic attention switching related to frontal generators [22]. The latter was also tested by Alain et al. by noticing a diminished temporal MMN amplitudes on subjects with prefrontal lesions [36]. Furthermore, there is a strong and reciprocal connectivity anatomically between auditory and prefrontal areas [37]. Numerous studies have found evidence for multiple generators of the MMN in the primary auditory cortex. Rinne et al. also showed that generators in the prefrontal cortex activate later than those in the auditory [20]. In this sense, MMN reflects a greater prediction error or mismatch between top-down predictions and current inputs. Obviously, an implicit increase in prediction error calls for an adjustment on the brain's internal model or memory of the stimuli. However, model adjustment itself lacks the explanation of the decreasing activity under standard sessions, it concentrates only on the deviance detection.

Adaptation hypothesis Jääskeläinen et al. (2004) challenged the previous hypothesis, suggesting that MMN was generated by a much simpler mechanism, neuronal adaptation in the auditory cortex of the brain, which would cause attenuation and delay of the N1 response [38]. The repetition of the same stimuli would cause a short-lived adaptation to non-novel sounds. The neuronal adaptation (spike-frequency adaptation) results from the activation of calcium-dependent potassium channels that lead to slow hyperpolarization, decreasing neuronal excitability and firing rate. Thus, adaptation is a local phenomenon that is independent of pre-synaptic mechanisms and rests on changes in post-synaptic responsiveness. This leads to a misidentification of the N1 wave. However, there are some

counter-examples also which cannot be explained by the adaptation hypothesis.

First, Winkler et al. (1997) states that it predicts the MMN duration and latency should match those of the N1, which has been shown not to be the case [39]. Secondly, MMN can also be elicited in the absence of N1 – either the subject is asleep or the stimulus is omitted [40]. Furthermore, infrequent decrements in tone intensity also evoke an MMN [41]. MMNs of this sort cannot be explained by local adaptation only suggesting that there is more complex neuronal mechanism involving more neuronal populations. Lastly, the temporal source underlying the MMN is located more anterior than the source underlying the N1 [42] meaning that they employ different neuronal populations [43].

Predictive coding Predictive coding (or, more generally, hierarchical inference in the brain) states that perception arises from integrating sensory information from the environment and our predictions based on a model of what caused that sensory information. The interaction between different cortical layers minimises the prediction error so that it can estimate the most likely cause of the input [44, 45]. Model adjustment fits in this concept as a marker for error detection, and MMN would be caused by the discrepancy between the auditory input and a memory trace embodied in top-down predictions. The prediction error then would be used to modify the model [33, 34]. Similar happens for predictive coding; the current inputs are predicted from previous inputs. The main difference is that during the repetition of subsequent events this prediction error is suppressed and thus the MMN disappears [45, 46]. In predictive coding each hierarchical layer compares the top-down prediction from the higher level with the actual sensory input from the bottom-up information. Higher areas make the abstract picture of the world whilst lower ones process the current input [47, 48]. Using backward connection higher levels try fit their predictions and lower ones attempt to reconcile the predictions from higher areas with the actual input via forward connections, a prediction error signal, i.e. information not predicted by higher areas [49].

With Bayesian statistics taken into picture, we have top-down prior $p(\theta)$ (θ being the inner parameters of the model) and a likelihood $p(y|\theta)$ (y being the input) based on maximising the posterior or conditional density $p(\theta|y)$. This provides a message-passing between levels where higher levels send top-down predictions and lower levels return bottom-up prediction error. When this converges, a multilevel representation is born, where there is a compliance on all hierarchical levels between the input and the prediction. Therefore, neuronal activity tries to suppress prediction error to represent the states of the world; this is perceptual inference [23]. Since hierarchical inference (e.g. predictive coding) rest on the relative influence of the top-down prediction and bottom-up prediction error, when a standard stimulus can be predicted more precisely by top-down afferents, less weight is

assigned to bottom-up information flow, thus post-synaptic responsiveness weakens. This is what adaptation hypothesis states, too.

1.6 Stimulus-specific adaptation and deviance detection

In accordance with the adaptation hypothesis, the act of habituation is present during the standards therefore resulting in a decreased neural activity to the same stimulus. Taaseh et al. showed the stimulus-specific adaptation in rat auditory cortex [50]. Stimulus-specific adaptation (SSA) (or repetition suppression – RS) is the specific decrease in the response to a frequent stimulus, which is not similar (or partially similar) to another rare stimulus (deviant).

SSA shares many properties with (but is probably not identical to) MMN. The first emphasises the adaptation of responses to the standard tone, whilst the latter concentrates on the responses to the deviant tone. A substantial effort has been to demonstrate that MMN is not (or not only) due to the rarity of the deviant, but is at least partially due to the violation of the regularity of the tone sequence caused by the presentation of the deviant [51, 52, 53]. Having a sound sequence in which many silent trials are shown and then a deviant comes with the same probability as in the traditional oddball paradigm is called a 'deviant-alone' control [51]. In these sequences there is presumably no regularity to break, and therefore the response should only reflect the rarity – in contrast with traditional oddball where the deviance is detected also. Though, due to the rarity also, the responses will be large because the auditory system is stimulated at a much lower rate. This problem is alleviated, but not fully solved by the 'deviant among many standards' control where the rate of the deviant is the same, but there are no special standards – the standard is replaced by many other stimuli [52, 53].

Furthermore, though SSA is believed to lie upstream of MMN, it has been shown that SSA does not depend on NMDA receptors, while MMN does. Thus, an emphasis should be put on the distinction between mismatch negativity and stimulus-specific adaptation in auditory cortex [54]. As a contrast to the previous, a study has shown that oddball sequences might engage true deviance-detection mechanisms, rather than only adaptation in narrow frequency channels, already at the level of auditory cortex [50]. There have been studies which also examine the role of SSA and deviance detection in MMN in other animals. For example, results based on macaques indicate stimulus-specific adaptation rather than deviance detection, and that the neural mechanisms reside in cortical areas outside of A1 [55].

Numerous studies on human ERPs using both types of control sequences have suggested that MMN is indeed an index of true deviance detection. Deviance detection has been

related to the occurrence of the MMN, evoked 100 to 250 ms after the occurrence of the deviant [56]. Taaseh et al. also have shown that the probability of a tone is the key factor to the strength of the response: deviant-alone, deviant and diverse conditions induced larger amplitude responses whilst high probability conditions (standard and equal probability) gave rise to smaller responses (hence the other name, repetition suppression and surprise enhancement) [50].

To distinguish the SSA from the real deviance detection mechanism, another method, the so-called "equiprobable" series was introduced, in which the deviant had the same probability as before, but now no standard is specified, i.e. the deviant is in a mixture of stimuli [52, 53, 57]. Whilst originally the MMN was defined as the difference between the deviant and the standard, the discrepancy between the deviant and the equiprobable series reveals a "genuine", surprise-related (visual) mismatch [58, 59]. The stimulus-specific adaptation is quantifiable through the comparison of standard and equiprobable series. A quick summary on the comparisons can be seen on fig 5. Though, there have been studies that still suggest the contribution of RS to MMN as well, [57, 60, 61] and other studies on non-human primates failed to show a surprise-related response to the violation of regularities [54, 55, 62]. Amado and Kovács have shown that the neural mechanisms behind visual MMN (on humans) are category dependent. The repetition suppression and surprise enhancement are responsible for different object categories; RS was the main component for faces and chairs whilst the other for the real and false characters [63].

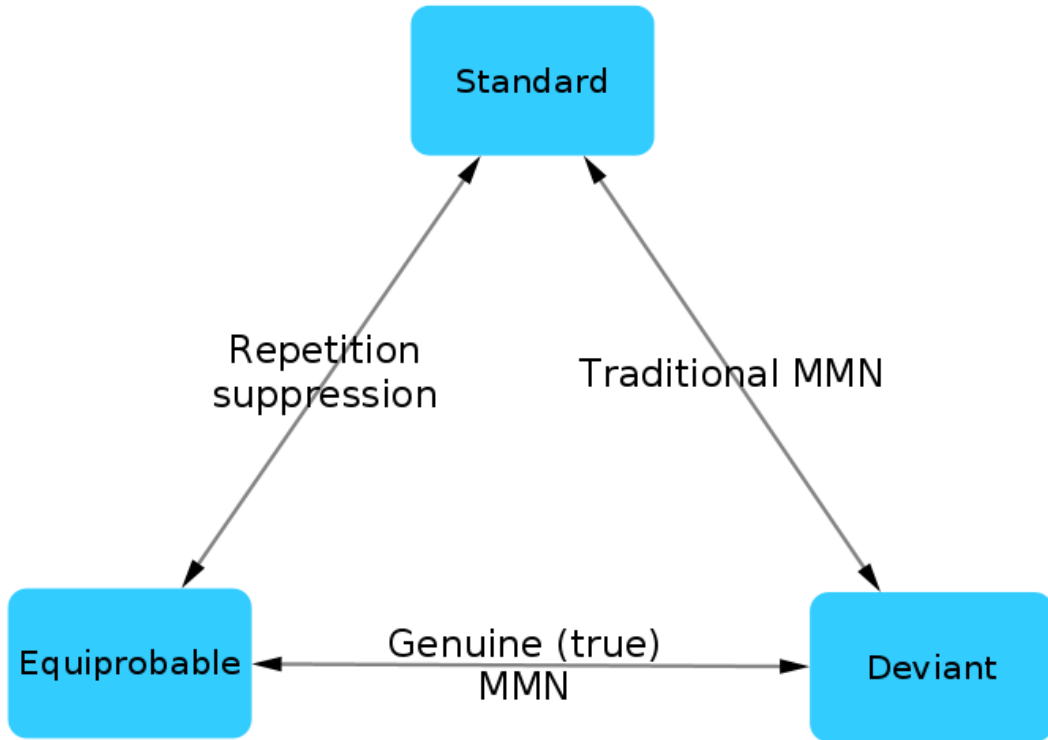


Figure 5. **Comparison graph.** The possible comparisons between the mentioned sequences and the connotation of their connecting edges. Here only those methods are present, which have been mentioned so far.

2 Experiment

The novelty our experiment carried in itself is that many of these phenomena had not been tested for multimodal stimulation. The experiment was done in Amsterdam at the Swammerdam Institute for Life Sciences, University of Amsterdam by Umberto Olcese and his team. There are still ongoing experiments by the time of writing this thesis which allows us to ask for modification on the experiment set based on our calculation results. Methods discussed in the following sections were guided by the preliminary results based on the data recorded from the V1 (primary visual) and the AL (anterolateral) cortices of one anaesthetised mouse.

Multimodal stimulus consists of a visual and an auditory stimulus presented at the same time for the same length – in our oddball paradigm. For the sake of simplicity, only two types of stimuli was shown for both of the senses. For the visual stimulus it was a sinusoidal drifting grating with 0.05 cycles/degrees (50 % contrast) either horizontally or vertically and static grating during inter-stimulus interval. On the auditory side, band-limited white noise was presented at about ~ 75 dB volume with either 8-12 kHz (low pitch) or 12-16 kHz (high pitch) frequency bands. Combining these stimuli together results in 4 different stimuli naming them A-D – see fig. 6. For the transparency, colour codes have also been associated with each. With this in hands we can not only evoke

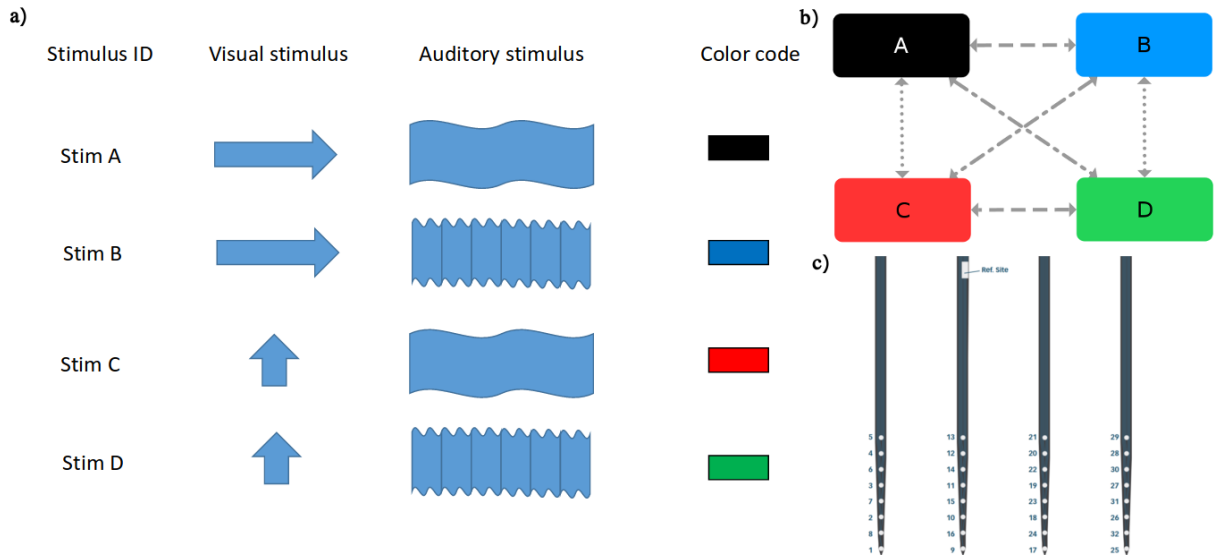


Figure 6. **Experimental background.** a) **Overview of the four different types of multimodal stimuli.** Visual stimulus means the direction of the grating whilst the auditory stimulus' pictograph refers to the frequency band (high pitch or low pitch). b) **Graph of mismatch types.** The mismatch types between the stimuli marked in the following way; dashed: auditory, dotted: visual, dashed and dotted: both (bimodal). c) **The placement of the electrodes on one device.** There is a reference site on the second shank. Please note that the numbering of the sensors is partially inconsistent, though, it was corrected in the later works.

separate visual and auditory mismatch negativity (vMMN and aMMN, respectively) but we are also able to make it conditional based on the other senses' inputs and, of course, the bimodal type.

During this particular recording 2 Neuronexus probes were placed in the V1 and AL area of the mouse with 32 sensors on each (32kHz sampling frequency). These were grouped onto 4 shanks with 8 recording sites having $100 \mu m$ between sites and $400 \mu m$ between shanks – see fig. 6/c). Three sessions have been done: the full MMN task, a deviant only control (where there were no standards, each stimulus was chosen with the same same probability), and a many standard control (where the same stimuli was shown consecutively but with 12 seconds of inter-stimulus interval – thereby the notation *modified inter-stimulus interval (M-ISI)*). The intuition for the latter was to somehow remove the memory trace part also. For further examination, one can extract only the first and last of each standard chunk – a standard chunk is the ensemble of few standard consecutive stimuli. By comparing the M-ISI to the deviant, it reveals the contribution of memory trace, and, by studying the relation between that and the standard one can study the role of the length of the inter-stimulus interval. However, the analogue for the equiprobable–M-ISI relation still remains unclear. An overview of the possible comparisons are on fig. 7. All the nodes (including the small ones in the standard) are capable of being in connection with any other, though, the figure only shows the relevant

ones, and since the first and last of every standard chunk are obviously the scions, they are not considered to be the main parts due to their limited numbers, i.e., to reveal the hidden connection between the beginning and the end of a standard and a deviant other, more sophisticated, more refined methods would be necessary.

All the data acquisition was carried out in MATLAB and was saved as .csc files. Due to the lack of resources, our team decided to handle and process the data in Python3, therefore resulting in a large number of pieces of codes to help converting those .csc raw data into normal, Python3-edible files. Furthermore, the executive team immediately performed a spike detection based on typical spike waveforms. The resulting data are the spiking times for identified individual cells, with what we can perform cellular-level comparisons also. The recordings are from mice and very few of them have been under examination more than once, with various anaesthetic levels. Furthermore, the recording areas also vary between different auditory, visual and anterolateral cortices and the number recording sites and sessions. What is common in all are the stimulus types.

For an example, the similar type of aMMN could be elicited by presenting Stim A as standard and Stim B as deviant or Stim C as standard with Stim D being deviant, but a conditional aMMN would only result from just narrowing these options onto one pairing (fig. 6/c.). Moreover, coupling the mismatches together would produce a bimodal mismatch negativity (bMMN), i.e., both the visual and the auditory stimulus differ for Stim A and Stim D.

The 3 sessions mentioned above took about one and a half an hour to conduct. Fig. 8./a) shows the length of each chunk in every standard session. The dots mean the length of the previous segment's length (in number of stimulus) and tell us that there was a minimum of 7 stimulus until no deviant could have come, resulting in a ($7 \times 2 =$) 14 seconds temporal distance between deviants. There are numerous 8 and 9 stim length chunks with a few of longer ones. The legends mean the total number of stimuli in each sequence and the x axis tells us the overall timeline in terms of timestamps. The vertical lines mark the type of each deviant stimulus. On the b) subfigure, the equiprobable and the modified inter-stimulus interval's temporal data acquisition is seen. What is important to note here is the difference between the timescales. Even though, the number of stimuli for each kind is equal between the upper and lower graphs, we took the octuple of the regular, 1.5 sec inter-stimulus interval which resulted in a ~ 16 minutes of total recording time as opposed to only ~ 2 for the equiprobable session. Furthermore, as the figure shows, the maximum number of consequent same stimuli is 2 during the equiprobable session, but for the M-ISI the stimuli were separated and shown after each.

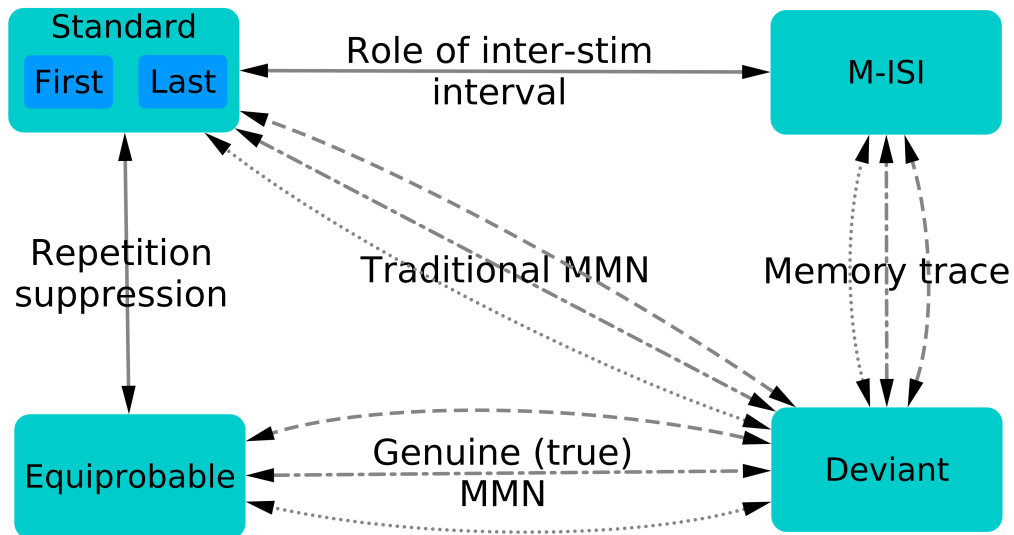


Figure 7. **Summary of the comparisons between the different sequences.** There is no adequate physiological explanation for the relation between the equiprobable and modified inter-stimulus interval (M-ISI) sequences, hence, it is not indicated on the picture. Since the first and last series can be derived from the traditional standards, they do not form separate sequences by themselves and finding relations between those and others are only secondary, their primary reasons are discussed in section 2. Different mismatch types are marked with varied lines also.

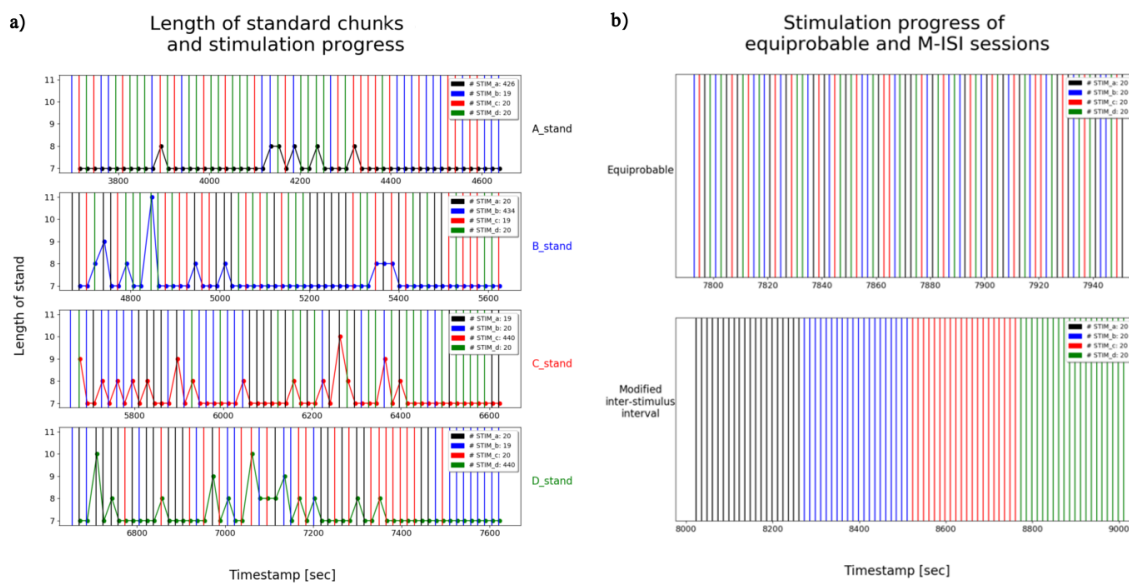


Figure 8. **Session progression.** a) **Full mismatch task.** The subgraphs show the length of the previous chunk measured in number of stimuli with dotted lines and the type of deviant stimulus with vertical lines for each standard sub-session. Legends show the total number of stimulus presentations whilst the x axis is intended to reveal the temporal evolution. b) **Equiprobable and M-ISI sessions.** Equiprobable and M-ISI sessions' temporal evolution with the presence of every stimulus (shown with vertical lines) are shown. It is important to note here the difference between timescales and the equality of total number of stimuli shown.

3 Data processing and evaluation methods

There are multiple ways to analyse the given dataset trying to maximise the obtainable information. First, a simple temporal, point-by-point testing is sufficient to reveal the most conspicuous signs of difference. Later, in Fourier space, we can begin to develop the methods by starting from cellular levels, then looking at cortical areas, and finally a channel-wise picture to find whether our conjectures were true or not. In this section, I am going to explain these methods including their relevance and how they guided us towards other measures.

3.1 Temporal evaluation

Beginning with the traditional point-by-point evaluation with hypothesis testing was the first milestone of our research. It is widely used and has a common ground in either confirming or confuting our ideas. The temporal evaluation consisted of carrying out a t-test hypothesis testing on all possible time-point during the stimulation – however, the first and last 10 milliseconds have been chopped off from the window due to on-off switching effects leaving us with a 480 milliseconds (15360 data-point) long series. Our null hypothesis was that the two ensembles are significantly different, therefore are from different distributions. It was a one-way testing, so only the discrepancy can be seen, but it is easier to quantify. This evaluation was executed on all possible channels (64), all methods (e.g. standard-deviant) and all mismatch types (auditory, visual, bimodal or none).

3.2 Spiking histograms

Thanks to the work of the Umberto Olcese and his team, we have the opportunity to take a look at the spiking times for all the identified neurons. The reason behind this method was to gather a phenomenological map about the distribution of cells and therefore identifying sources of signals. No statistical hypothesis-testing and no comparison have been done.

The presence of stimulus-specialised neurons have been mentioned in many articles (most interesting one is the so-called *Skywalker neuron*) [64]. This suggests that identified neurons may show specialisation signs for our stimuli. Just by looking at the frequency histograms, we try to find out whether these neurons were nearby to any sensors or not. Furthermore, the overall activity of the cells and their placements may give further information about the sources of signals. However, these are not the only cells that were present, just the identifiable ones, thus, other origins may form the overall activity otherwise.

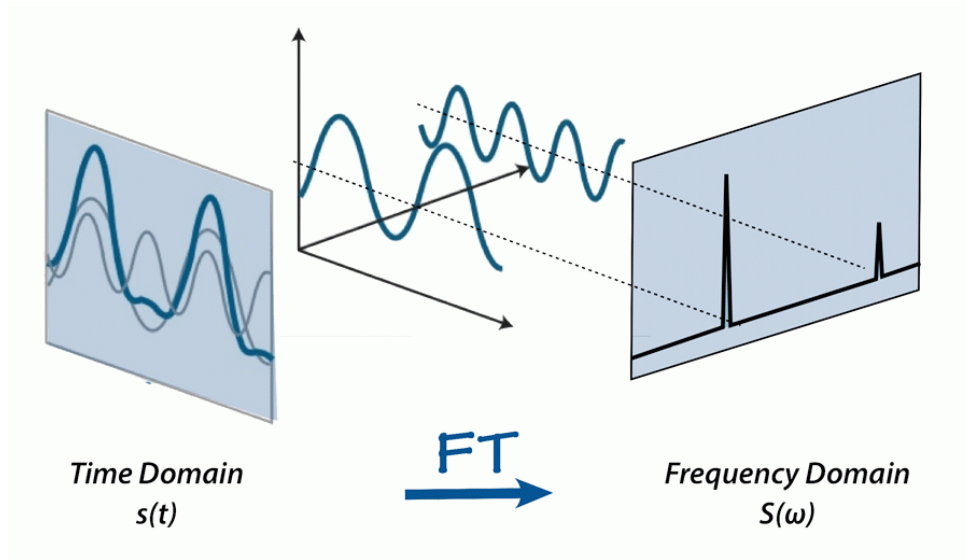


Figure 9. **Fourier transform.** Two sinusoidal waves added together in time space, are perfectly separated as two spikes in frequency space. The conversion between them is done with Fourier transform (FT). Figure source: aavos.eu.

3.3 Frequency map

3.3.1 Frequency conversion

Next step was to combine the information of the channels and the ability to analyse the frequencies together in order to get an overall view of the activity of all the channels. In the previous section we counted the number of the spikes and divided by the total length of stimulus to get a nominal, firing frequency for a given cell. However, the channels measure not only the spikes but the overall activity of multiple circuits resulting in an extensive Fourier spectra. Frequency components of a given temporal signal can be obtained by the following expression (Fourier transform of a time series($F(x(t))$)):

$$X(\omega) = F(x(t)) = \int_{-\infty}^{+\infty} x(t) e^{-i\omega t} dt. \quad (2)$$

Equation 2. shows how to generate the Fourier components at a given frequency ($X(\omega)$). Absolute magnitude of these complex numbers tells about the amount of that frequency present in the original function. Phase however, represents the offset of the basic sinusoid in that frequency. Since real life recordings are not continuous, to calculate these components, we used the discrete Fourier transform (DFT):

$$X[k] = \frac{1}{N} \sum_{n=0}^{N-1} x[n] e^{-i2\pi \frac{n}{N} k}, \quad (3)$$

where $X[k]$ is the discrete Fourier component in the k th bin, $x[n]$ is the n th element of the original discrete time series which has a length of N . In order to determine what the k th bin means, let us turn to the Nyquist–Shannon sampling theorem:

$$f_N = \frac{f_s}{2} = \frac{1}{2\Delta t}, \quad (4)$$

which generates a sufficient condition for a sample rate (f_s) that permits a discrete sequence of samples to capture all the information from a continuous-time signal of finite bandwidth. In eq. 4. f_N denotes the upper limit for frequency, and δt means the time between the samplings.

The result of an N -point DFT is an N element complex vector and for strictly real data, only the first $1 + N/2$ bins matter, as the others are a redundant complex conjugate image. Dividing $F_s/2$ by $N/2$, and you get $\Delta f = F_s/N$ as the frequency spacing of $1 + N/2$ equally spaced DFT results, including both end points, DC and $F_s/2$.

3.3.2 Creating map

By having Fourier spectra for all stimuli and types, one can create an average of them. In this section, we omit the phases and keep only the absolute magnitude for each one, thus we can create an ensemble for each type and method. These ensembles create a great base for statistical comparisons: in each frequency bin, one can compare the distribution weights and using the tools hypothesis testing decide whether a significant difference is present or not. One-way Student's t -test have been used during the whole procedure with respect to the Bonferroni-correction. The same methodological comparisons have been done here, which are listed in fig. 7.

Furthermore, we created a guidance for frequencies which serves as a level of trustworthiness. During DFT the signal is supposed to be periodic and to reduce the edge-effects a window is used on them. If only one cycle is present in the signal, then it will be more affected by the window as it would have three, i.e, whilst having 3 cycles, the middle one is less deteriorated in contrast to only one cycle. To reduce this effect a longer epoch time would be necessary, but since our stimuli had a fixed length of 500 ms and we crop 10 milliseconds after and before the ends our best choice is to create a marker around a critical frequency under which less then 5 cycles were possible. This f_{crit} critical frequency is around 10.5 Hz ($5 \times \Delta f = 10.42\text{Hz}$)

3.4 Coherence of cortical areas in frequency bands

Based on the results of the frequency map, we decided to calculate the coherence within frequency bands. Coherence as a measure of similarity between two signals in frequency domain. In this subsection, I am going to elaborate on cross-correlation, power spectral

density, coherence. Later, the formulation of measures is going to be discussed.

Neuronal oscillations and their inter-regional synchronisation is believed to be one of the mechanisms that enables interaction between various brain regions. To identify which regions are interacting or independent at any period of time and to analyse the connectivity we measured the coherence of the signals. Quantifying synchrony using EEG data has become a popular approach to study functional brain connectivity and like many other methods, coherence only tells us whether two regions are linked or not. Therefore, this measure is symmetric.

With $x(t)$ ($x[n]$) and $y(t)$ ($y[n]$) being temporal (discrete) signals, the (discrete) cross-correlation function $R_{xy}(t)$ is defined by

$$R_{xy}(t) = \int_{-\infty}^{\infty} x(\tau)^* \cdot y(t + \tau) d\tau, \quad (5)$$

$$\left(R_{xy}[n] = \sum_{m=-\infty}^{\infty} x[m]^* \cdot y[m + n] \right), \quad (6)$$

where $x(\tau)^*$ denotes the complex conjugation. Cross-correlation is a measure of similarity of two series as a function of the displacement of one relative to the other. If one computes the cross-correlation with the same signals, they get the auto-correlation function $R_{xx}(t)$. Autocorrelation, is the correlation of a signal with a delayed copy of itself as a function of delay.

Using the Fourier transformation on the cross-correlation function gives us the cross power spectral density $S_{xy}(\omega)$ defined as

$$S_{xy}(\omega) = \int_{-\infty}^{\infty} R_{xy}(t) e^{-i\omega t} dt = \int_{-\infty}^{\infty} \left[\int_{-\infty}^{\infty} x(\tau)^* \cdot y(t + \tau) d\tau \right] e^{-i\omega t} dt. \quad (7)$$

The same applies for the discrete cross power spectral density

$$S_{xy}[k] = \sum_{n=0}^{N-1} R_{xy}[n] e^{-i2\pi \frac{n}{N} k} = R_{xy}[n] = \sum_{n=0}^{N-1} \left[\sum_{m=-\infty}^{\infty} x[m]^* \cdot y[m + n] \right] e^{-i2\pi \frac{n}{N} k}. \quad (8)$$

By Fourier transforming the autocorrelation function we get the power spectral density $S_{xx}(\omega)$ and its discrete counterpart $S_{xx}[k]$.

The squared coherence $\gamma_{xy}^2(\omega)$ is defined in the following way [65]:

$$\gamma_{xy}^2(\omega) = \frac{|S_{xy}(\omega)|^2}{S_{xx}(\omega) S_{yy}(\omega)}. \quad (9)$$

For discrete signals we will use the following definition for coherence on multiple signals [66]:

$$C_{xy}[k] = \frac{|\langle S_{xy}[k] \rangle|}{\sqrt{\langle S_{xx}[k] \rangle \langle S_{yy}[k] \rangle}}, \quad (10)$$

where $C_{xy}[k]$ is the coherence in the k th frequency bin, and averaging is done through the trials (~ 20 for a given deviant). (Note that now we used the square root of the upper previous definition for continuous signals. In essence these are similar.) Due to this limitation, x and y can only be signals from the same sequence but can vary in channels. Since we had plenty of frequency bins and channels, during the evaluation we averaged in terms of frequency bands and channels in cortical areas.

4 Results

This section tells us about all the observations we made on the data. Trying to be concise and straightforward, though, the amount of results might suggest otherwise. The basic motive was to keep the data grouped in such a form, that on type of mismatch negativity is on one figure with one cortical area.

4.1 Temporal evaluation

The evaluation was discussed briefly in sec 3.1. Here, I want to elaborate on the methods I used. First and foremost, the point-by-point Welch-testing was done with a desired α value of 0.05, to get a confidence level of 95%. If there was only one comparison each set of data, then we would reject all those p-values which are lower than this threshold. However, Multiple comparisons require a Bonferroni correction to overcome [67]. This problem forces us to use a stricter (if not the strictest) threshold to reject our null hypothesis. The lower threshold is calculated by dividing the normal one with the number of data points in one set, which gives us the final α value, the threshold of $\alpha = 0.05/(480 \times 32) \approx 3.26 \cdot 10^{-6}$. This low of a threshold permits only those tests which do have an inner meaning, while not excluding the possibility of other significant differences either.

The first step was to run the significance t-test. Our null hypothesis was that the difference is zero. On fig. 10. one arbitrary channel's response and its stacked histogram is visible (the channel is from the primary visual cortex, V1). The signals are the average ERPs' difference for the traditional (deviant-standard) mismatch type and the lines above them mark the significant difference, i.e., the difference is surely non-zero. On the upper left corner, the auditory mismatch is seen – the equivalent comparison with 7. figure is the dashed edge between the standard and the deviant. Since we could create

Raw signal differences for the traditional MMN on channel 31

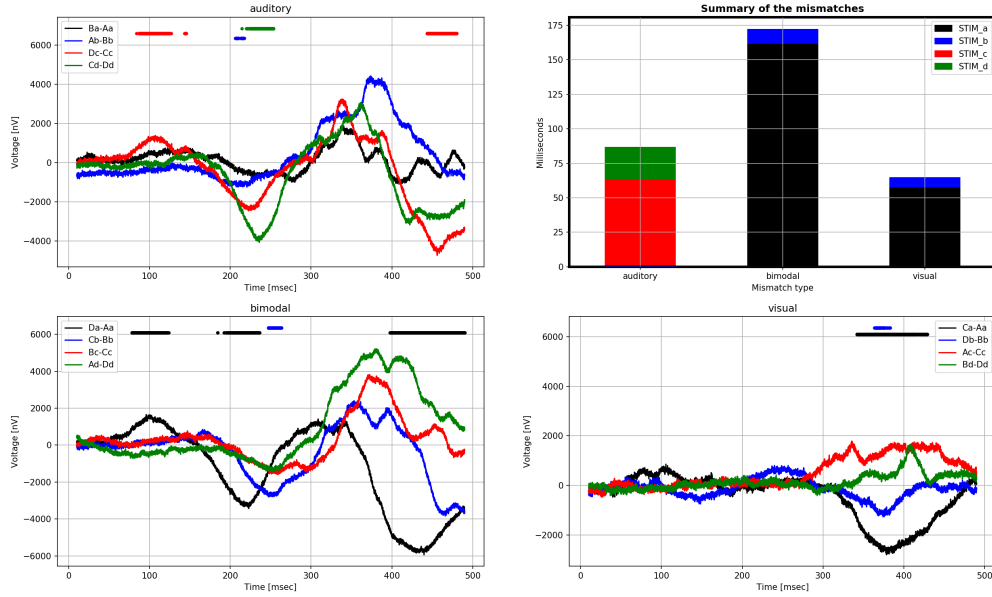


Figure 10. **Raw signal differences for the deviant-standard comparisons.** It is an arbitrary channel in the V1 cortex showing how the evaluation was constructed. Different temporal signal differences are shown in 3 sub-figures with the marking of significant ones (from the zero) using the Bonferroni corrected value of $\alpha = 0.05$. The top right box shows the stacked histogram of total length of difference for the three types.

4 examples from the auditory mismatch (see the mismatch-graph, fig. 6/b)), we have 4 different ERP differences: when the A was the standard and B was the deviant compared to the ERP from the sequence where B was the standard ($Ab - Bb$), vica versa ($Ba - Aa$), and of course for the other pairing also ($Cd - Dd$, $Dc - Cc$). Colouring always means stimulus type of the deviant, not the standard session. ERPs from this kind show that the most points for significant differences is from the C stimulus, where it was embedded in in an oddball sequence of D-s ($Dc - Cc$), one negative component (which is relative) around 100 ms from stimulus onset and another positive around 460 ms. Furthermore, the opposite of this oddball setup ($Cd - Dd$) produced the second most different signal having a positive peak around 240 ms, and there was a little bit of difference in response around this time for the stimulus A also ($Ba - Aa$). No significant difference is visible for stimulus B at this low of α value ($Ab - Bb$). A summary of this figure is seen in the box right next to it. The *auditory* bar shows the total length of different sections summed up. The dominance by the red (stim C) is visible, with some blue at the bottom and more green on top resulting a total of ~ 85 ms of different phase (out of $4 \times 480 = 1920$ ms possible time). However, this channel showed a greater discrepancy between signals for the bimodal mismatch governed mainly by the A stimulus' deviance during stimulus D ($Da - Aa$). A smaller portion to the stack is also given by stimulus B during standard C ($Cb - Bb$) marked with blue. On the mismatch-graph (fig. 6/b) it is equivalent with

the dashed-dotted edge between the standard and the deviant. The two main factors the visual mismatch were also the A and B stimuli.

By only having one-way comparison for the ensembles, it is easier to quantify the total number of different time points for one session and type, though, we did lose the information about whether the signal increased or decreased during that particular period. A basic assumption was also made while using these methods which is the following: the different time-points tend to band together, rather than follow such a distribution that would create separate points. This assumption is based not only the fact that different valleys and peaks have been shown in previous studies, but also having such a low α value would also prohibit the existence of single-point differences – averaging over many samples would vanish unexpected spikes in LFP away. Nevertheless, this particular figure (and especially the histogram) was created in such a way that different types of MMN are seen, but since our main goal is to find distinction between different methods (traditional, genuine and M-ISI mismatch) the grouping of the data will be shown in other ways.

To reveal the layer-specific connections and differences between methods, see figure 11. This figure shows the stacked histograms of the different time points for all the channels in the V1 during auditory mismatch. The numbering of the channels are corrected in such a way, that now the real places are visible, and the numbers mean only mean the order the device it named them. For easier identification, I decided to leave them as they are. Please note that these 32 channels are labelled from 1 to 32, but figures about the anterolateral cortex show numbering from 33 to 64, so that it easier to identify. Furthermore, there are all in all 8 figures (auditory, visual, bimodal mismatch and none for two brain areas) but only this one is in the body text, the other 7 are in the appendices in section A. However, as I warned the reader before, the grouping is different, therefore the bars now mark the methods, not the types of the mismatch which are listed below.

- **Traditional mismatch:** (deviant–standard) this was aimed to create the ground truth for the old type of mismatch used in oddball sequences about multimodal stimulation. This type of mismatch is believed to consist of both the surprise enhancement and the effect of withdrawal of the stimulus-specific adaptation.
- **Genuine mismatch:** (deviant–equiprobable) the genuine mismatch is the novel type of mismatch in which the deviant is compared to a sequence when the probability of the stimulus was the same, but no standard was given, disentangling stimulus-specific adaptation (SSA) from the MMN.
- **Role of memory trace:** (deviant–M-ISI) by comparing the deviant to a sequences where the inter-stimulus interval was many times larger one can determine the role of the memory trace, since there is no *echoing* left in the cortex during ISI giving us

the pure learning itself. It is a rudimentary initiative to disentangle the withdrawal effect of SSA from the MMN.

Stimuli dominance First and most obvious clue is the dominance of red and green colour (stimulus C and D, respectively): irrespective of the method used, where there is significant difference, the most of it comes from these two stimuli (and from the first especially). Negligible amount comes from stimulus B (blue) on channels 20 (row 2 – from top to bottom, column 3 – from left to right), 31 (r 5, c 4), 24 and 32 (r 7, c 3 and 4) and none from stimulus A (black). The cause behind this can be two main options: there is an effect, *conditional mismatch negativity*, that causes the brain to respond only to those auditory mismatches where the visual stimuli was vertically grating. This effect is either layer-specific (see below) or comes from another part of the brain involving more complex mechanisms. Another explanation on this phenomena is the inevitable fatigue. Since the deviants and the standards were all recorded at the end of the traditional MMN task (see fig 8.) it is possible that the anaesthetic state of the animal had changed (therefore the cognitive state and brain activity also) during this one hour long session. The same chromatic effect is visible at the anterolateral cortex (fig. 33.).

Cortical activity Nonetheless, lower cortical electrodes show an increase in different points for stimulus D also, which makes this area more active than the middle (3.-4. rows) or the first two sensors. Note: though the rows in this figure do not equal to cortical layers, the vertical spacing between the sensors allows us to approximate. Further elaboration on how the true neural activity was distributed among the channel is at the spiking histograms.

Methodical differences Another interesting thing to note here is the relative sizes of the bars. Despite from a few exception the traditional and genuine bars are in the same order of magnitude and for the lower middle part (5.-6. rows) the memory trace's bar is also similar; they follow such a pattern that genuine showed the highest activity, then the traditional and finally the memory trace. Explanation behind this can be that the repetition suppression did cause the neurons to fire at lower activity (than they did during equiprobable) causing the amplitude of the overall signal to decline. Therefore not just the average of the ERPs are lower, but also the standard deviations of the ensembles also, hence, causing the Welch tests to produce a higher α value, i.e., more (precise) measurements (~ 440 for standard and ~ 20 for equiprobable and M-ISI) then would lead to the sharpening of the edges of the positive peaks and negative valleys.

Number of significantly different time points
for auditory mmn
in the V1

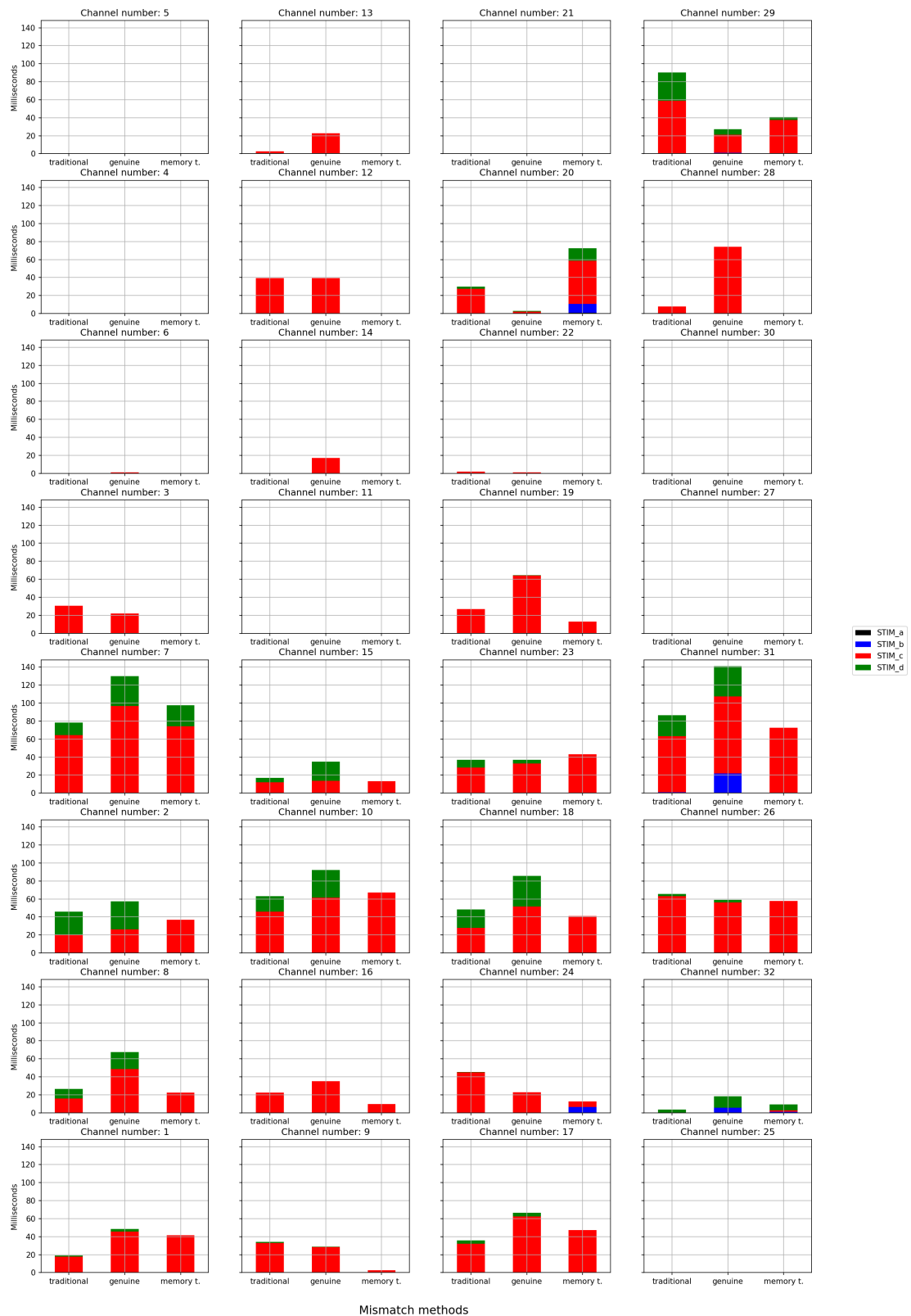


Figure 11. The length of significant differences for the auditory mmn in the primary visual cortex (V1). Different stimulus types are noted with different colours and the stacked bars mean the mismatch methods. Level of significance was the Bonferroni corrected value of $\alpha = 0.05$.

Comparing with other histogram maps As I mentioned before, the rest of the results are in section A. The former three paragraphs on the thoughts about the evaluation can all be found for the others – non-mismatching comparisons later.

- **Stimuli dominance:** the huge presence of one signal is visible for all three types of mismatches; blue (deviant was stimulus B while D was the standard) for the visual (fig. 30. and 34.) and black (D standard, stimulus A) for the bimodal (fig. 31. and 35.) The common point in all these is that one part of the values for comparison was recorded during D standard. It is still possible that these are truly caused by the strong presence of stimulus specific adaptation for the stimulus D as a standard making the others to increase the number of significant different points. On the other hand, for the auditory mismatch, it was not only visible for the D, but also for the C standard, which had happened before, indicating the factor of fatigue again.
- **Cortical activity:** All the figures in sec. A.1 show the same results (in spite of neural activity) as I discussed before: lower middle cortical electrodes are more active than others and channels on the top also produce more significant difference than the middle ones. Figures in section A.2 are similar, too, in that sense that the same cortical patterns of activity is visible for all the three mismatch types. Though, main differences are the higher activities in the deepest and the shallowest sensors.
- **Methodical differences:** The (relative) size of the bars are the same for the brain areas for the auditory and bimodal also. Only the visual mismatch produced different results for the methods. Here, memory trace bars are always higher and sometimes those are present only. One explanation behind this is the following: as the animal fatigued, the anaesthetic state has changed, caused the animal to weaken up, which would result in the increment of visual perception. This presence of visual perception would allow the animal to form a visual memory trace during the repetitive appearance of standard D chunks. The resulting deviants would carry this information inside, and when compared to a sequence lacking this feature, reveals the role of memory trace.

Continuing from the last point, one might ask that if the presence of such a memory trace is so crucial, why does not the equiprobable series show an increase also? To understand this, take a look at the non-mismatch comparisons at the appendices. In these figure now genuine refers to the repetition suppression (standard-equiprobable) and memory trace refers to the role of inter-stimulus interval – reminder: fig. 7. The dominance of the blue (stimulus B) is clearly visible suggesting that these areas were mostly occupied by neurons sensitive to this type of stimuli, however, at the primary visual cortex (V1) the presence of stimulus A for the equiprobable proposes that the main driver for these effects is the horizontal grating stimuli (visual stimulus). Cortical activities by electrodes are similar also. One type of explanation for the fact that the inter-stimulus interval

changed the activity more than equiprobable series, is that simply the presence of memory trace governs the overall signal more than the deviance detection. For further results, an experiment with an increasing length of ISIs (not just two) would be necessary.

The two main hypotheses that we proposed are not excluding. Conditional mismatch negativity and the fatigue of the animal may be connected to each other. There is a possible scenario that the decrease of anaesthetic depth of the animal's conscious state gives the possibility of the brain to form more complex thoughts, to permit the emergence of conditional mismatch, meaning that this phenomena requires higher abstractions in perception. Luckily, our colleagues in Amsterdam have conducted multiple experiments where not only the animal was different but the measured cortical area and the order of tasks also.

4.2 Spiking histograms

Spiking histograms only show the absolute value of spiking frequency. Spiking frequency was calculated by counting together all the spikes that had happened during the given time-window (10ms after onset and 10 ms before offset resulting in a 480 ms window-length) and dividing that number by the total length of stimulus presentation ($480 \text{ ms} \times \text{number of stimulus presentation} - \text{approx. } 20$ for a given deviant in one standard run). No inclusion of inter-stimulus spikes are present.

The have an overview about the total distribution of the cells between the sensors, please take a look at figure 12. This image shows the number of identified cells on each channel with a pie chart indicating the distribution of all spikes between the neurons. Radii of these objects are proportional to the natural logarithm of the total number of spikes found on one channel – a division by ten is done for scaling. Ordering of the segments and colouring are also based on the number of spike for one neuron. It is important to note that one cell is dedicated to only one channel, no overlaps are permitted.

For example, on channel 13 (row 1, column 2) the number of identified cells is four, having one that is the most active covering more three quarters of the whole pie chart, i.e., more than 75% of all the spikes found on channel 13 are from one single cell. Furthermore, the second most active cell on this particular sensor covers nearly all of the remaining part leaving only a small, hardly noticeable area for the rest. Reasoning behind this includes that channels having identified neurons are more governed by the signal of these, whilst temporal data with no dedicated cell is believed to measure rather the overall potential of a population of many cells. Radius of this chart larger than channel 29, but smaller

Number of identified clusters (62 in total)
and the distribution of spikes (V1)

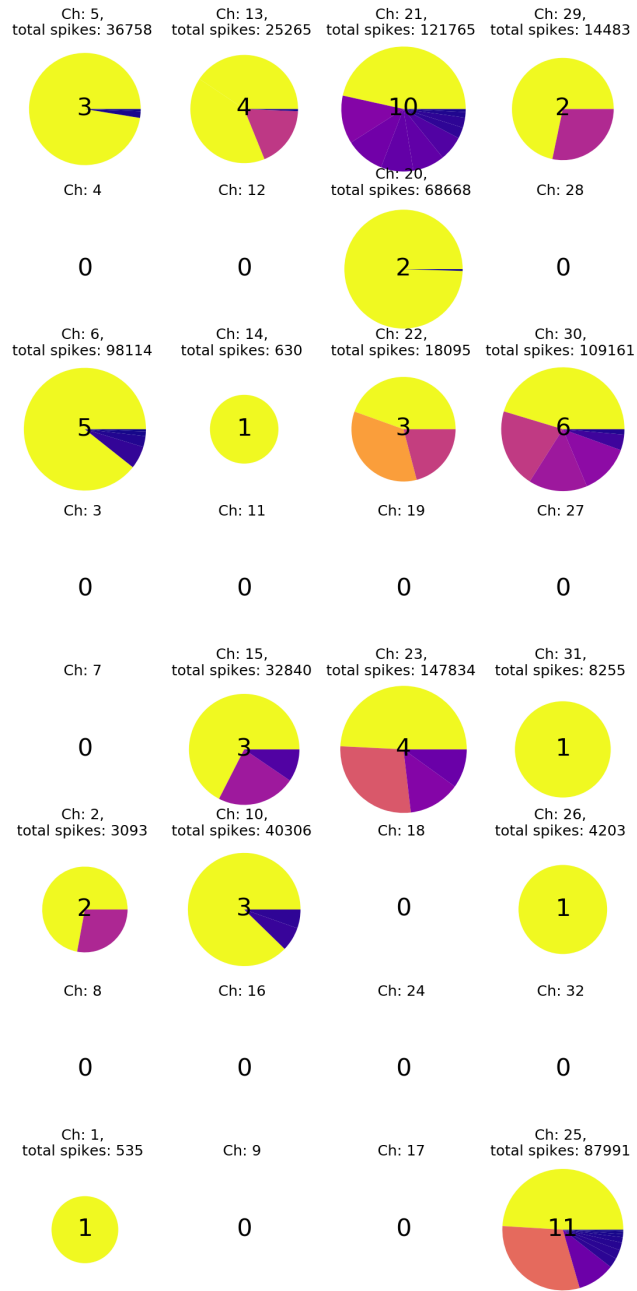


Figure 12. Number of identified cells on one channel and the overall spiking activity at the primary visual cortex (V1). Radii of pie charts are calculated by dividing the natural logarithm of total number of spikes detected on a given channel by ten (for scaling). Colouring of these objects are based on the number of spikes for one cell.

than channel 5 and 21 indicating a rather average size (amongst all).

No cells have been found in the fourth and seventh rows, and by excluding those (with the others consisting zero neurons), the average number of cells on one channel rises from 1.94 to 3.65. Most of the channels share more than one cell and approximately at least half of the all spikes came from a one. This allows us to dedicate a *dominant cell* to a channel: a dominant cell on a channel is the one which has the highest activity of all. The interesting thing here to notice is the layer-like structure. Two rows are empty, suggesting that there is a drastic change in the density of neurons, i.e., it is possible that empty rows indicate the border of layers, since sensors vertically are spaced with having $100\mu\text{m}$ in between. Though, the size of the soma of a neuron ranges from 4 to 100 micrometers in diameter.

If we take a look at fig. 37 at the appendices, the average number of cells on a given channel is 0.41 and 1.63, respectively. The figure shows the same setup for the anterolateral cortex. This low number can be caused by multiple things, including unfortunate placement, noise, movement of the device, etc. One unusual cell is found channel 62, having a high activity compared to others. Nevertheless, the dominant cells for this area can also be found in the same way.

4.2.1 Dominant cells

Using the definition mentioned above, we can analyse further the activity of the most dominant cells by separating the spikes by stimulus- and mismatch types. I want to emphasise once again that only those spike were counted, which had happened during a stimulus, so that, if a cell was more active during the inter-stimulus interval, it is not shown in the figures.

For the dominant cells in the primary visual cortex (V1), see fig. 13. The figure shows the bar chart of the different mismatch methods and types. Bars show the average frequency for a given type with the colour meaning the portion of a given type of stimulus being shown. The six bars are the following (from left to right): auditory (aud), bimodal (bim), visual mismatch (vis), same (standard sessions), equiprobable (equip) and M-ISI (modified inter-stimulus interval). Bars not reaching 2 Hz for all are the cells which fired unevenly, having less than ~ 2160 total number of spikes which is the number total number of stimuli.

First thing to notice here is the variety of frequencies present. Not only the most active neuron ever (channel 21) but also the lazy ones are seen having more than 23 thousands spikes and less than a hundred for the whole experiment. This can be explained by the

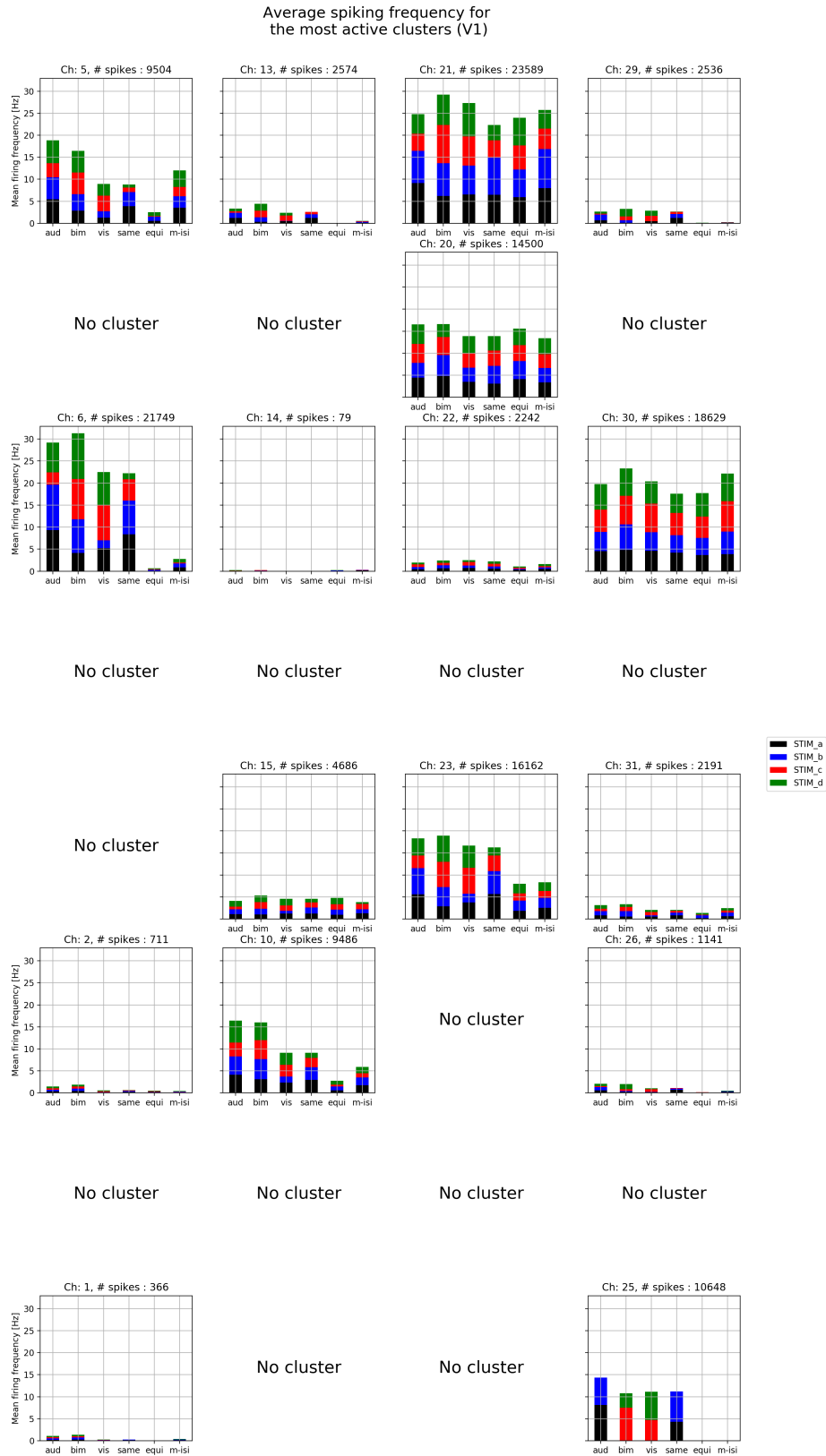


Figure 13. Average firing frequency for the most active cells on each channel at the primary visual cortex (V1). Bar charts are shown according to real-life placements, channel numbers are ids. Colours are consistently defined by the stimuli – see figure 6. Y-scales are shared across all axis and the total number spikes are noted within the titles.

presence of excitatory and inhibitory cells. A typical excitatory cell (pyramidal cell – which mostly occurs in the hippocampus) is possible to fire at low, even at 1 Hz frequency and have an location-based activity with a thinner typical spiking waveform. On the other hand, inhibitory neurons are not location-based, tend to fire at high frequencies (even 80 Hz) and have a thinner waveform. Furthermore, knowing the order of sessions done, the relative size of the bars are meaningful. If we take a look at channel 5, 6, 13, 25 and 29, the effect of fatigue/SSA is clearly visible: on the fourth bar, the relative height of the C and D standard (red and green, respectively) is smaller. Since we know that during the longest session (full MMN task, see 8.) the C and D standard sub-sessions followed each other at the last, the firing rate decreased due to the declination of excitability which is either a cause of stimulus-specific adaptation or fatigue. By analysing the results for the equiprobable and M-ISI sessions, contentious deductions can be made: there are neurons which were affected by the fatigue (channel 6, 13, 23, 29), i.e., bars for both the equiprobable and M-ISI sessions remained short. Others were either capable of resting (ch 5, 10) or kept firing frequency (15, 20, 21, 22, 30, 31) regardless of session and stimulus type.

One interesting dominant cell is the one on channel 25: bars here show pronounced both stimulus type- and method-specificity. Starting point: no equiprobable or M-ISI firing happened, meaning that it is only happened for the standards. But which standards? From the "same" bar we can conclude that none of the firings happened during C or D standards. Furthermore, stimuli A and B were an auditory mismatch and since the "same" bar is lower (probably due to auditory stimulus-specific adaptation) we can conclude that the visual stimulus played a significant role. But since we have do have firings for the bimodal and visual mismatch also this can only be a *signalling cell*, that fires regardless of type of visual stimulus. Nevertheless, lack of firing during later sessions is ambiguous. To entangle this, let us take a look at the second most active cells in V1.

As fig. 14. shows, those channels which had only one cell, now are empty. The reason behind this is by using the first two most active cells, we cover at least three quarters of the total number number of spikes. Once again, no cells with less than ~ 2160 spikes are analysed due to insufficient data. Elements based on the previous discussion can be found here. Doubtfully, channel 6 and 13 show fatigue-like signs, though, the visual and standard bars also remained short, but channel 30 showed similar spiking frequency despite the methods or stimulus types. Channel 21 showed lower average spiking frequency for auditory mismatch and standard session; nearly halved keeping the same distribution for the stimulus types, it is probably a visual deviance detection cell. Just similarly for the dominant cells, the second most active source on channel 25 shows interesting, not easily classifiable results. Equiprobable and M-ISI spikes are barely visible, and though the sizes of the other bars are smaller (different scales from the dominant cells' chart) the colours are the *quasi-inverse* of each other. Other colours are

present also, but the averages are mainly governed by the previously mentioned stimuli. Since it these two neurons are relatively close to each other (are on the same channel) it is either a result of misclassification of spikes, these two are the same in real life, or these are two separate cells, being part of a larger circuit and each others' contraries, i.e., one spikes, when the other not.

Dominant cells at the anterolateral cortex are worth mentioning also, figure 38. shows them. Most of the neurons were not so active, except for channel 62. Despite the relatively high average frequency of the bars, it is quite obvious that this cell rather shows the effect of fatigue, than any other. Other cells were not active enough, therefore the second most active cells are not worth to plot.

4.3 Frequency map

The generation of the frequency map is similar to the one at the temporal evaluation at the beginning. We created the raw Fourier signals and used point-by-point Welch test with Bonferroni correction to determine any basic difference between the ensembles. Furthermore, considering biological conditions (maximal known firing frequency in the primary visual cortex for mice is 582 Hz) we chose to reject the maximal possible Nyquist-Shannon frequency (16kHz) determined by their sampling theorem and used all data up to 1 kHz [68]. Thereby our significance test can still produce the same assurance with higher threshold. Using a rudimentary α of 0.05, and only the first 480 frequency bins (generating an upper limit of 1 kHz) with the correction the final α value, the threshold decreases to $\alpha = 0.05/480 \approx 1.042 \cdot 10^{-4}$.

Codes To help understanding the notation for a given sequence, let us define a code for them. A code always consists of one capital and one small letter; e.g., the code for the sequence of stimulus B recorded during the standard session of A (therefore getting an auditory mismatch) is *Ab*. Similarly, the conversion works vice versa, the code *Bc* means that series of stimulus C which was recorded during the standard session of B (bimodal mismatch). For the equiprobable and M-ISI session we will use the *E* and *M* notation, respectively. Comparison then is indicated by having a colon sign between the codes: *Ad:Ed* means that the bimodal deviant series of stimulus D (so that it was presented during A standard session) is being testing against the series of D stimulus whilst it was embedded in the equiprobable session. Comparison codes with different small letters (different stimulus types) are meaningless. Also, the order is arbitrary, since the statistical test only determines whether the difference is non-zero or not.

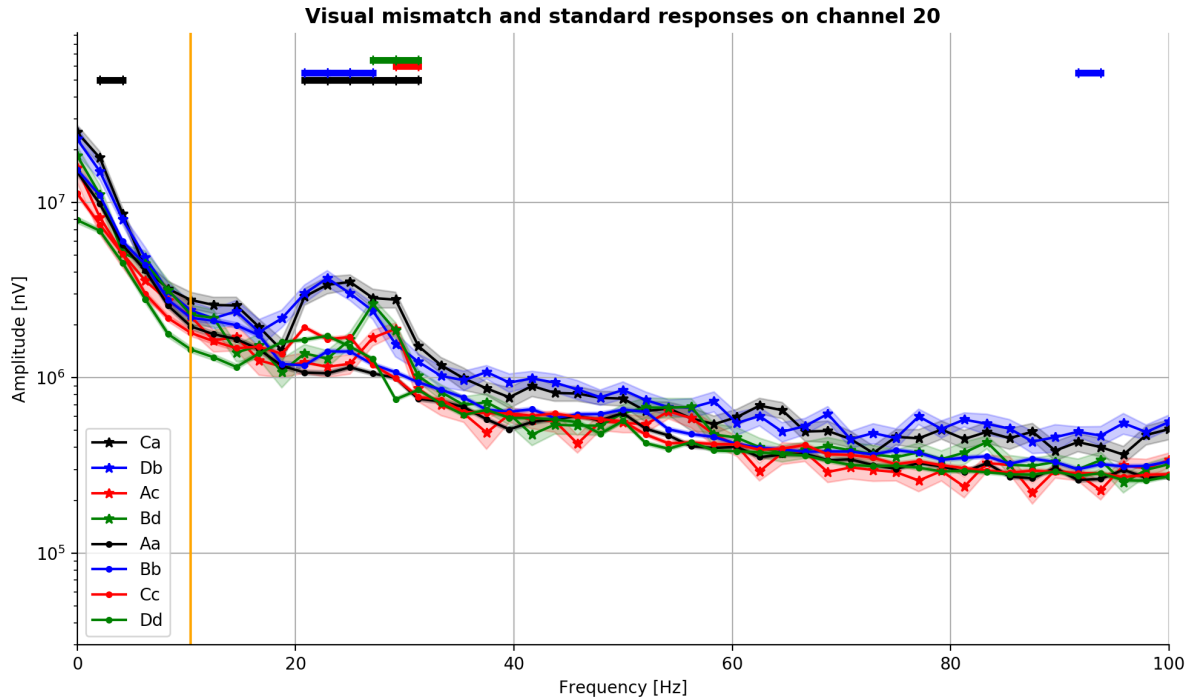


Figure 15. **Logarithmic average Fourier spectra for the traditional visual mismatch and the standards on channel 20.** Shaded areas around the lines are the standard deviations. Significant differences are indicated as lines above them and a vertical frequency marker is in orange for reliability. Level of significance was the Bonferroni corrected value of $\alpha = 0.05$.

4.3.1 Average Fourier spectra

Figure 15. shows the average amplitudes for each frequency bin with the shaded areas being the standard deviation. Two ensembles are presented in this graph: the visually deviants (having codes Ca, Db, Ac, Bd, marked with lines and asterisk) and their corresponding standard sessions (same capital and small letters, marked with lines and dots). Colouring is consistent with previous figures, defined in section 2. Furthermore, on top the significant differences are shown having the same colour. The already mentioned frequency reliability marker line is with orange colour.

Decreasing amplitudes are caused by the pink noise ($1/f$ noise). The presence of pink noise in acoustic terms means that each octave carry the same amount of power. Furthermore, biological systems tend to show bifurcative self-organizing system, and have cyclic symmetry with infinite degrees of freedom, and stationary random stochastic processes characterize their dynamism. Any kind of white-noise electromagnetic excitation (like "electrosmog" in general) is filtered by the biosystem, and it gives a characteristic pink-noise answer-signal to this excitation [69]. On fig. 39., we also noticed this kind of signal governing our data. The noise from the Brownian motion is also presented, as a scale. Please note that the lines representing the noise are not fitted, just multiplied with

an arbitrary number so that it would match more with the data.

Analysing fig. 15. suggests two observations: first, there is a significant peak around 25 Hz, and second, there is a noise that governs the spectra. To elaborate further on the noise, please see sec. C. in the appendices, where the cause of this phenomena is explained briefly. This plot shows the amplitude of each frequency bin on a semi-logarithmic scale. Since we use frequency bins the significant differences mean around 2 Hz so that particular peak for the Ca line (black with asterisk) has a width of 10 Hz between 20 Hz and 30 Hz (5 bins), roughly. A narrower peak is visible in this region at lower frequencies for the Db mismatch and at higher frequencies for the two others. Now we can conclude that during multimodal stimulus the traditional visual mismatch is present in the primary auditory cortex. Furthermore, the Ca and Db shows that those kind of deviants show larger differences where the visual vertical grating was the standard and the deviant was the horizontal. The inverse of this is less present but still there. Another important note here is that these two pairings (Ca and Db) are also higher in amplitudes even in high gamma regions while the others are more likely to their standard sessions.

To check whether other kinds of mismatch types are present on this channel, please refer to fig. 16. Auditory and bimodal mismatches are shown along with the repetition suppression (equiprobable-standard) in the top right box. For the auditory mismatch, there is a significant difference in the beta region for those mismatches where the visual stimulus remained vertically grating. This suggest the presence of *conditional mismatch negativity*, where one type of MMN emerges only when the other is in a given status. The peak between 20 and 30 Hz has nearly vanished and in higher frequency regions there are no spectra that is always greater than the other. Nevertheless, this small presence of conditional auditory mismatch in the primary visual cortex does have a contribution to the bimodal mismatch also. Though the significantly different regions did not add up simply, the numbers of each have risen. The peak has shrunk only between 20-26 Hz, but other differences have appeared in lower beta regions for the A and B stimuli (which had none during only visual mismatch). Just like during visual mismatch, the Da and Cb (wich had a visual switch from vertical grating to horizontal grating) are the one with the most significant differences and are higher in amplitude also in greater frequency regions. The same dominance goes for these two stimuli for the equiprobable-standard comparison also. Even though for this comparison that particular peak has translated to lower frequencies and shrunk further, the higher activity for all stimulus types during equiprobable are also present. Now we can conclude the following points:

- **Visual mismatch:** albeit the presence of traditional visual mismatch in the primary visual cortex is a non-novel information, it is great milestone to reassure ourselves

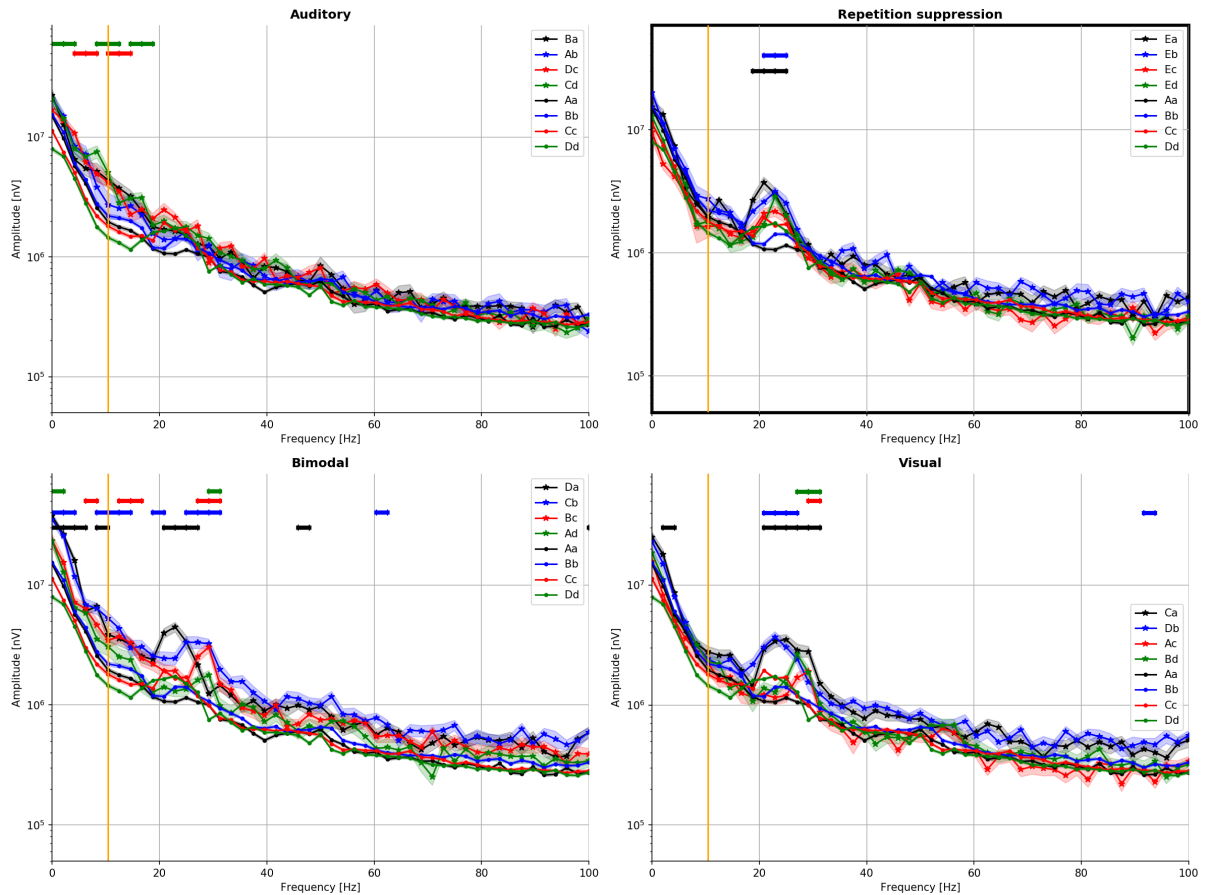


Figure 16. **Average Fourier spectra examples.** Three types of traditional mismatch (deviant-standard) with the repetition suppression (equiprobable-standard, top right box) on channel 20. Significant differences are marked with lines above them, the frequency reliability line with orange is around 10 Hz. Level of significance was the Bonferroni corrected value of $\alpha = 0.05$.

and note that this phenomenon is stronger for particular, one-way changes than vice versa.

- **Conditional mismatch negativity:** the emergence of auditory mismatch upon particular visual stimulus is a novel phenomena in terms of multimodal stimulus. To further investigate this, we need to look at other channels/animals.
- **Bimodal mismatch:** stimulating and detecting the brain with bimodal signals is also a non-novel thing [70]. Here we have an indication of how the separate visual and auditory mismatches added together influence the elicited bimodal MMN.
- **Repetition suppression:** repetition suppression is also visible on this particular channel and has effects on the ERP regardless of stimulus type.
- **Location of differences:** it is also notable that most of the significant differences are not distributed equally on the frequency scale but rather form peaks or groups

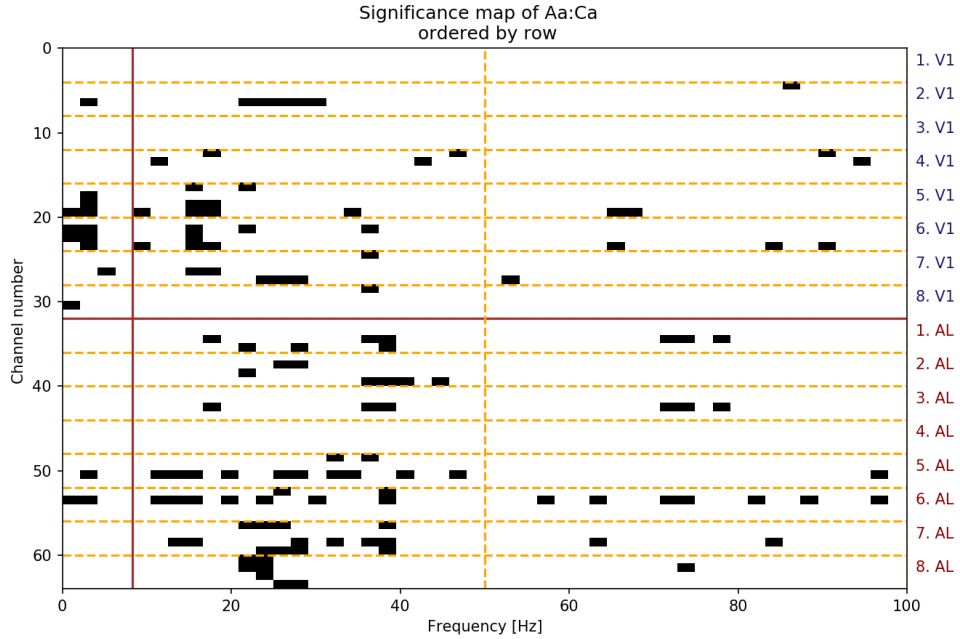


Figure 17. **Example of a frequency map.** The single-coded significance frequency map for one kind of visual mismatch. The map is ordered by row so four channels are in the same row (orange horizontal grid). Level of significance was the Bonferroni corrected value of $\alpha = 0.05$.

in the beta and gamma region. With this in hand, we can use our assumption on quantifying the differences to get a broader picture of the cortex.

4.3.2 Creating frequency map

So far, we only used one channel's response. In the following, we will switch to the representation of frequency maps so that all of the channels' information is visible. These maps only show the significant differences, they do not show the absolute value of the frequency components.

Figure 17. shows an example on how frequency map works. Horizontal and vertical axes mean the frequency bins and the channel numbers. The first 32 channels are from the primary visual cortex (V1) and the other half is from the anterolateral cortex (AL) separated by a brown horizontal line across the map. On the right hand side, the corresponding rows are shown for each area with increasing depth with orange, horizontal, dashed lines helping as a grid. The brown vertical line around 10 Hz is the reliability frequency and the orange at 50 Hz marks the mains frequency for most European countries. What we have seen on fig. 15 as black peak 20 and 30 Hz is now represented as a black line in the second V1 row at the same frequencies. Fig. 18. also shows us the significance map but now with Ac:Cc comparison on it also. The end of

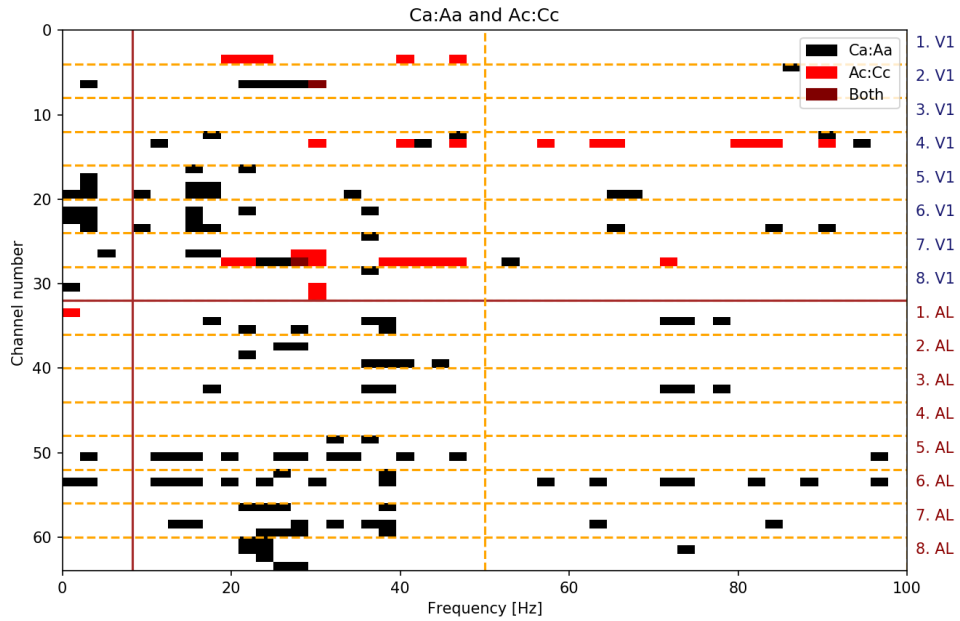


Figure 18. **Example of a double-coded frequency map.** The map is ordered by row so four channels are in the same row (orange horizontal grid). Now the codes are the inverses of each other so there was a difference in both directions, the marker is coloured in both ways. Level of significance was the Bonferroni corrected value of $\alpha = 0.05$.

the peak is now dark red which means that there was a significant difference in both directions. Notice that the inverse direction is only present in the primary visual cortex for reliable frequencies, i.e., red markers are only in the V1 above 10 Hz. Next, our step is going to be to visualise all of the possible frequency maps for a given mismatch type.

4.3.3 Visual MMN

First, let us take a look at fig. 19. which shows us the frequency maps of visual mismatch for all the methods. Stimulus types are paired together making two columns, and rows mean the methods. Markers on each map are the same as discussed previously.

Traditional MMN What we have seen in the previous subsection, the presence of traditional vMMN, is also true for the whole cortex. All of the four stimuli as deviants elicit differences in frequency bins, however, only the A and B stimuli are those which are able to create them in the middle-deep, 5-6-7th row in the V1 and in the anterolateral cortex also. Differences in the AL are present in the lower rows of electrodes, but they do not show frequency-specificity. The two others were able to elicit different frequency components in the shallowest and deepest electrodes of V1.

Visual mismatches

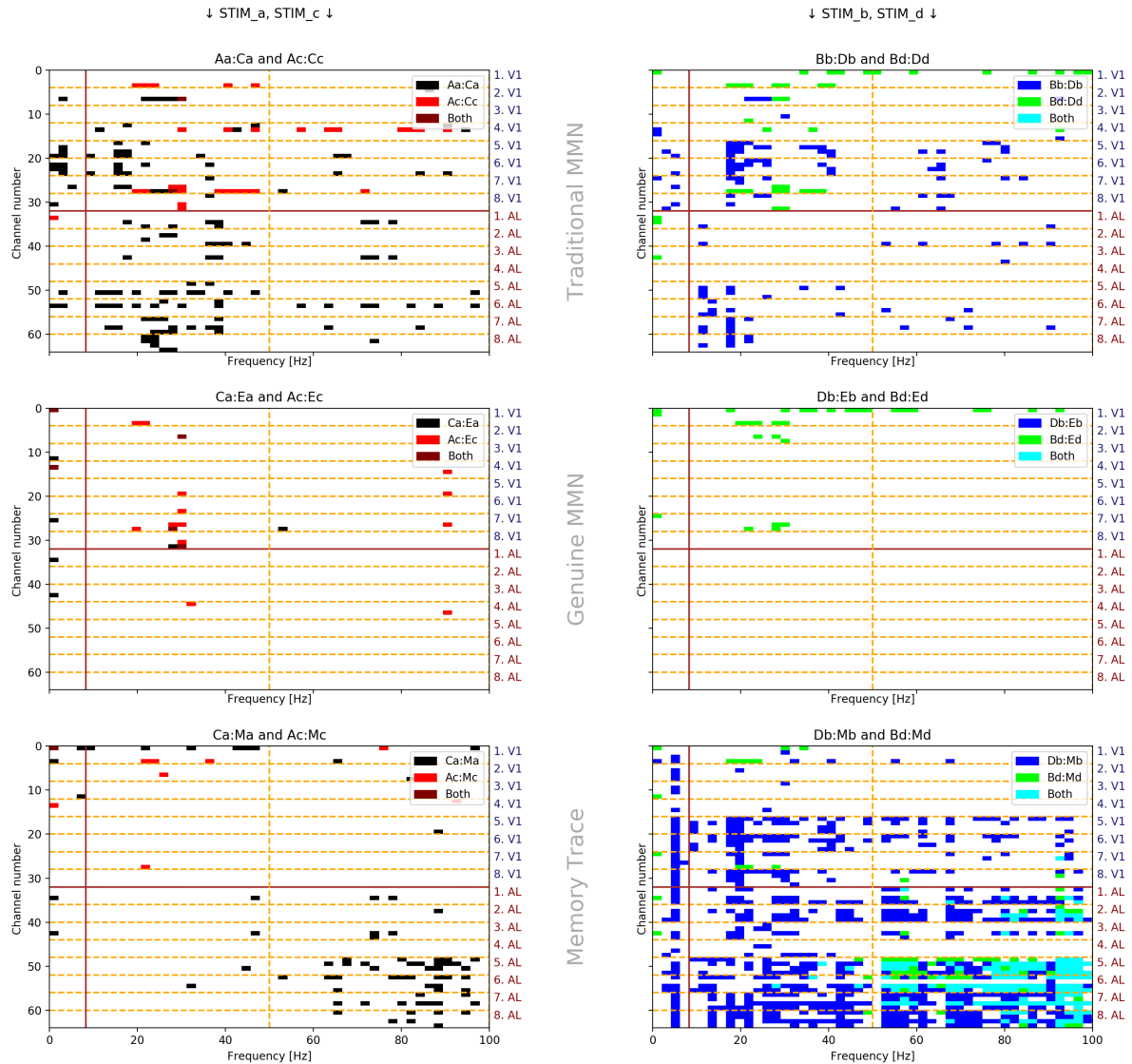


Figure 19. **Visual frequency maps.** The frequency maps for all the possible visual mismatch for different methods. Rows mean the methods and columns separate the stimuli so a sporadic conditional mismatch is visible. Level of significance was the Bonferroni corrected value of $\alpha = 0.05$.

Genuine MMN But what was less visible for one, more valuable for the other; even though stimuli C and D were *only* able to create differences as such, for the genuine MMN those are still present, unlike the others. This suggest a massive stimulus-specific adaptation for stimuli A and B. Despite for two frequency bins for stimulus C, anterolateral cortex has shown no difference for this method.

Memory trace During the memory trace experiment, the anterolateral cortex was more active and the appearance of differences in higher gamma frequencies suggest the activation/inactivation of other cells or group of cells. However, the the fact that most of

the differences came from those comparisons which had one part taken during the C and D standards also suggests the appearance of fatigue, once again.

4.3.4 Auditory MMN

Fig. 20. shows us the frequency maps of auditory mismatch for all the methods. The same setup is visible here, rows contain one method whilst columns contain one stimulus pairing.



Figure 20. **Auditory frequency maps.** The frequency maps for all the possible auditory mismatch for different methods. Rows mean the methods and columns separate the stimuli so a sporadic conditional mismatch is visible. Level of significance was the Bonferroni corrected value of $\alpha = 0.05$.

Traditional MMN Mismatches created with this method show that only stimuli C and D were able to elicit such ERPs that were significantly different from their standards. However, we cannot ignore the effect of fatigue, once more. Nevertheless, those electrodes in which the phenomenon is present, are the same as the ones for the visual MMN: the lower middle electrodes of V1 show significant differences for both directions in nearly all frequency bins under 50 Hz, but above it stimulus C is the dominant. Dominance for stimulus D is visible in lower beta frequencies at the shallowest sensors of V1 (1, 2, 3). The deepest electrodes produce significant changes also in this frequency band, but for both directions. Furthermore, the anterolateral cortex shows these changes up to 60 Hz for the upper electrodes, as opposed to only 40 Hz for the others.

Genuine MMN For the genuine MMN, lower middle electrodes of V1 show significant differences in the beta region, whilst others only in the lower beta for stimulus A. In the anterolateral cortex, lower sensors also showed differences sporadically. For the two other stimulus types, what is notable is the reduction of significant differences for the stimulus D. By that, which was yellow for some, now turned red. There is no change in the structure of significant differences whatsoever.

Memory trace The main effect of memory trace is visible in the anterolateral cortex. In the lower middle regions differences in high gamma regions have appeared for all stimuli except for C. Causes of this may include the activation/inactivation of other groups of cells. For other parts in any of the cortices, stimulus D has disappeared, which is either due to the effect that the modification of ISI does influence the elicitation of MMN or the fatigue, since the signals for those comparisons which remained are partly from the D standard sub-session.

4.3.5 Bimodal MMN

Frequency maps for the bimodal MMNs are shown on fig. 21. The setup is the same as before.

Traditional MMN Despite some overlap, the two pairings show the emergence of traditional bimodally stimulated mismatch negativity in different regions of the visual cortex and frequency bins. For easier analysis, please take a look at fig. 40. in the appendices, which tells us about the layer-specific distribution of the bMMN. Stimuli A and B elicit more differences in the higher beta regions (V1) than below 20 Hz, regardless of placement of sensors. However, stimuli C and D have a much higher influence on the lower middle electrodes, such as the former produces differences in the lower beta band, whilst the latter does this to the upper. In the anterolateral cortex, the higher sensors show an important difference in low gamma frequency band for stimuli A and B, seldom they do

Bimodal mismatches

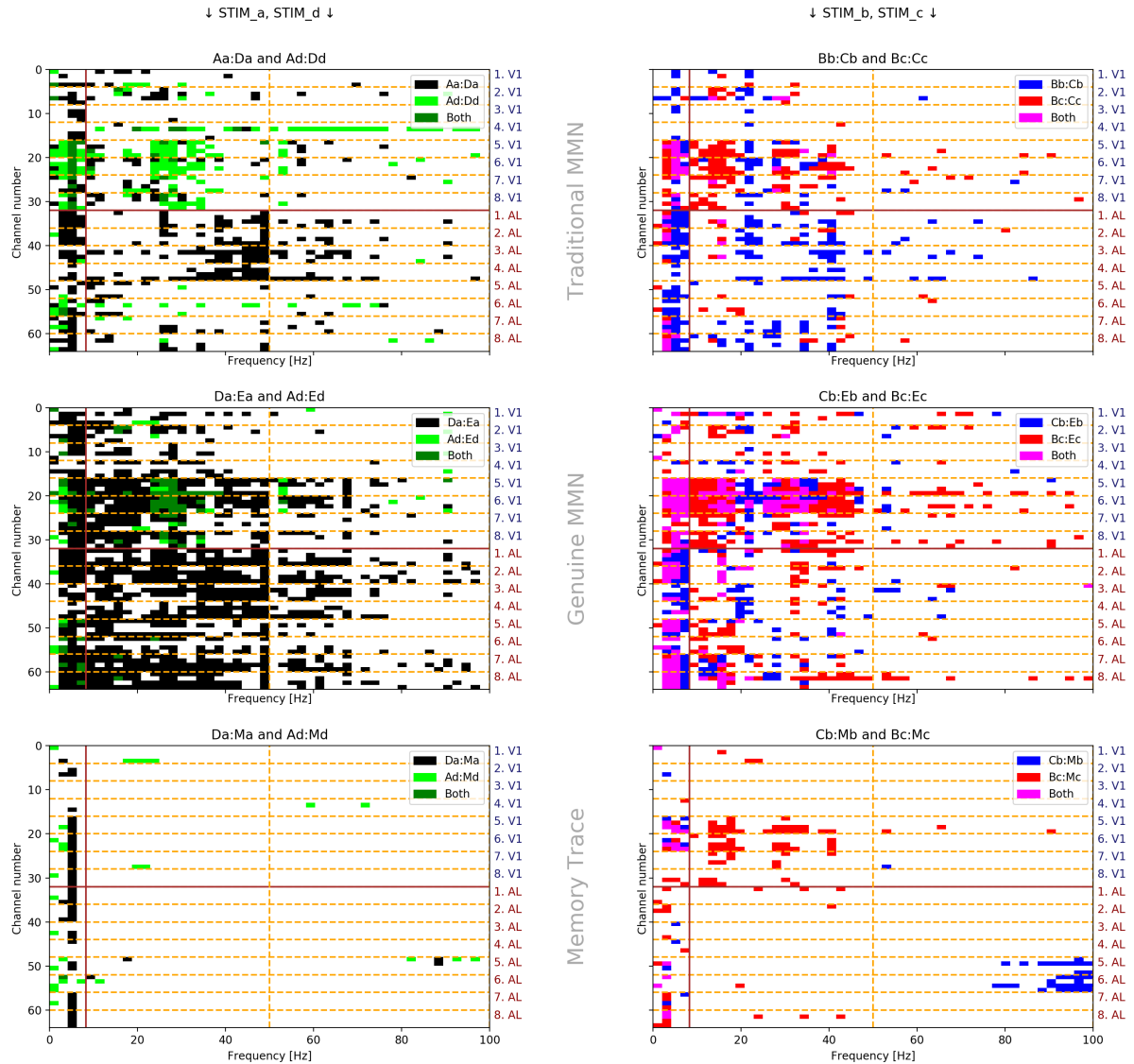


Figure 21. **Bimodal frequency maps.** Bimodal mismatch frequency maps for different stimulus type pairings and methods. Level of significance was the Bonferroni corrected value of $\alpha = 0.05$.

for C and never for D. Furthermore, deeper electrodes of AL are modified by all of the stimuli sporadically.

Genuine MMN First thing to notice is the presence of black, the colour of stimulus A as a deviant embedded in an oddball sequence of D standard being compared to its equiprobable equivalent. Despite the higher sensors in V1, all channels are affected more or less by this comparison. However, what are common in both sub-figures are the elicited differences in the lower middle electrodes around 30 Hz. We can call this phenomenon the *genuine bimodal mismatch negativity*. In the anterolateral cortex, stimulus A is dominant

but stimuli B and C are present also, whilst there is no sign of significant change to stimulus D.

Memory trace In the primary visual cortex (V1) only stimulus C was able to elicit differences, nonetheless, that happened for that particular lower middle electrodes. Furthermore, except for that stimuli, all the others show varying amounts of differences for higher gamma band in the lower middle sensors in the anterolateral cortex.

4.3.6 Non-mismatch comparisons

Non-mismatch comparisons are those which do not contain the deviant signals, see fig. 22.

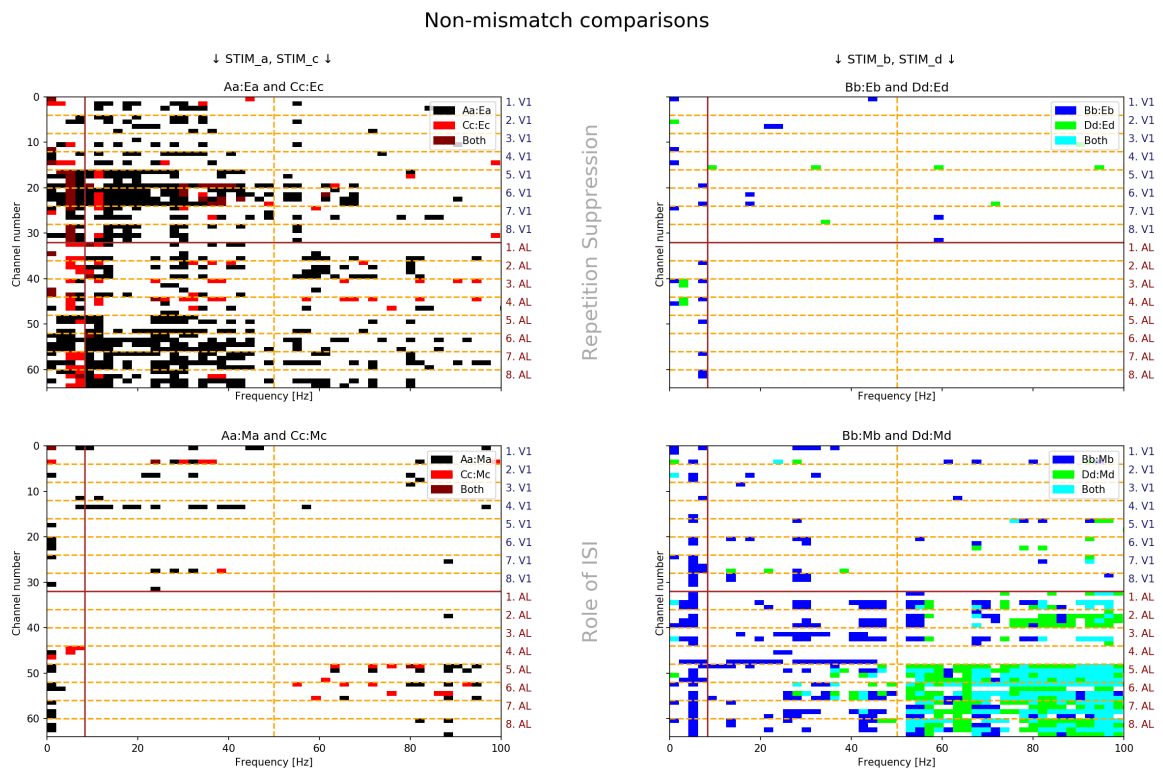


Figure 22. **Frequency maps of non-mismatch comparisons.** Pairings of stimuli is purely based on better understanding, with no deeper meaning. Level of significance was the Bonferroni corrected value of $\alpha = 0.05$.

Repetition Suppression Significant differences for the repetition suppression developed only for stimuli A and C. Supposing that equiprobable is the base and due to repetition the signals of the standards do not increase (see fig. 16.) we can conclude that there is a stimulus specific adaptation for stimuli A and C in terms of bimodal stimulation both in the primary visual (V1) and anterolateral (AL) cortex. This effect is present only sporadically for the other stimuli in the V1 and missing in the AL. Interesting to note also, that while stimulus A affects the electrodes on the lower half of the AL, stimulus C does this to the higher ones.

Role of ISI To determine the role of inter-stimulus interval for the mismatches, we compared the standards to a sequence where this parameter was larger. Please note that there were more than 440 standard signals and only 20 M-ISI recordings. The emergence of difference for all stimuli in higher frequencies in the deeper AL sensors is present here also. To determine the relation of signals, please head to the appendices and take a look at one channels response to these to sessions on fig. 41. Please note that the frequency limits have changed so we can conclude that the trend that shows higher activity during M-ISI session is eroded for larger frequencies. However, the M-ISI stimuli increases the activity higher in gamma bands for deeper AL electrodes. Stimulus B was able to produce this in lower frequencies also. In the visual cortex few differences are present, with no evident structure.

During this method we noticed that many phenomena happened within frequency bands. To analyse the connectivity inside and between the cortical areas, we will use coherency.

4.4 Coherence of cortical areas in frequency bands

As it was mentioned before, calculating the coherence between channels can help us analysing the connectivity further. Figure 23. shows an example on coherence between channel 64 and other channels from AL (red) and V1 (black) during stimulus A during the standard session of D (bimodal mismatch). Each frequency band and colour will be represented as the average of them, i.e., the values between 10 and 20 Hz for all the red lines will shrink to their spatial and frequency-based mean. This particular plot will be shown later as 10 values: 5 bandwidths with 3 types of coherence (cross for those which are not in the same region and V1 and AL are treated separately).

Knowing the bands which define the averaging over the frequency bins, figure 24. explains how spatial averaging works. The a) image shows an example on how coherent the channels were during stimulus A under the standard session of D in the (22,45) frequency range. Lower triangle matrix is shown since coherence is symmetric. Channels are reordered by rows meaning that the first 4 channels are located uppermost, the second group of 4 are one step lower and so on. Dashed red lines separate the upper half from the lower whilst the filled one marks the border of the devices. Upper and lower small triangle matrices are from V1 and AL, respectively. The square in the bottom left corner marks the cross-coherence, where the term *cross* refers to spatially separated channels. b) figure shows the values after taking the spatial average over the regions. The colourmap is defined in such a way to help the reader avoid any association with stimulus specificity.

Even though the coherences may vary between channels and sessions, given our setup, we can analyse the difference between them. Using violinplots one can not only represent

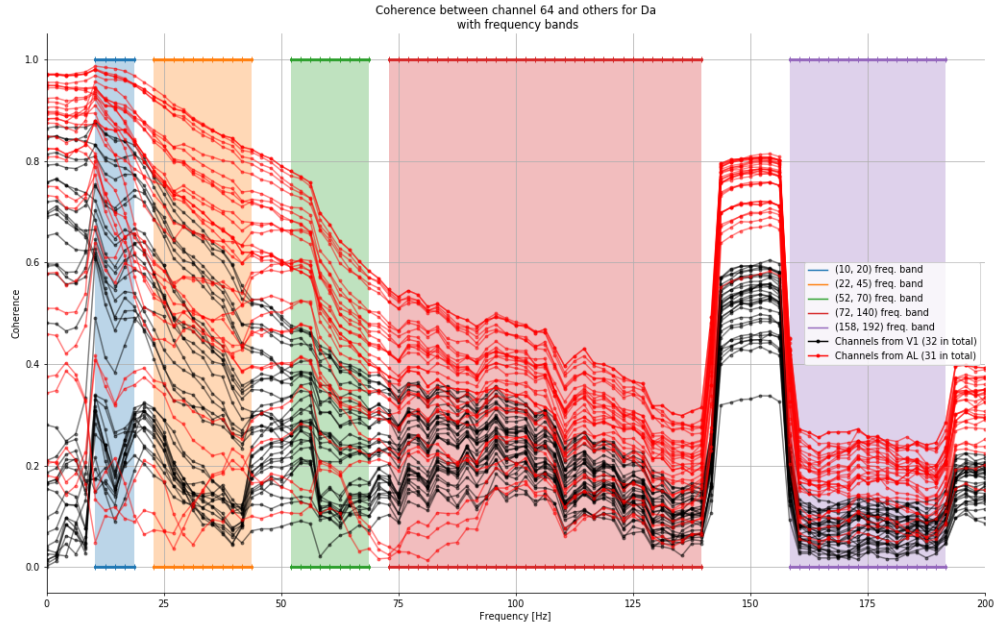


Figure 23. **Coherence between channel 64 and other channels for Da sequence with the bands.** The figure shows the value of the frequencies between channel 64 (from AL) and other channels (31 channels from AL marked with red and 32 channels from V1 with black).

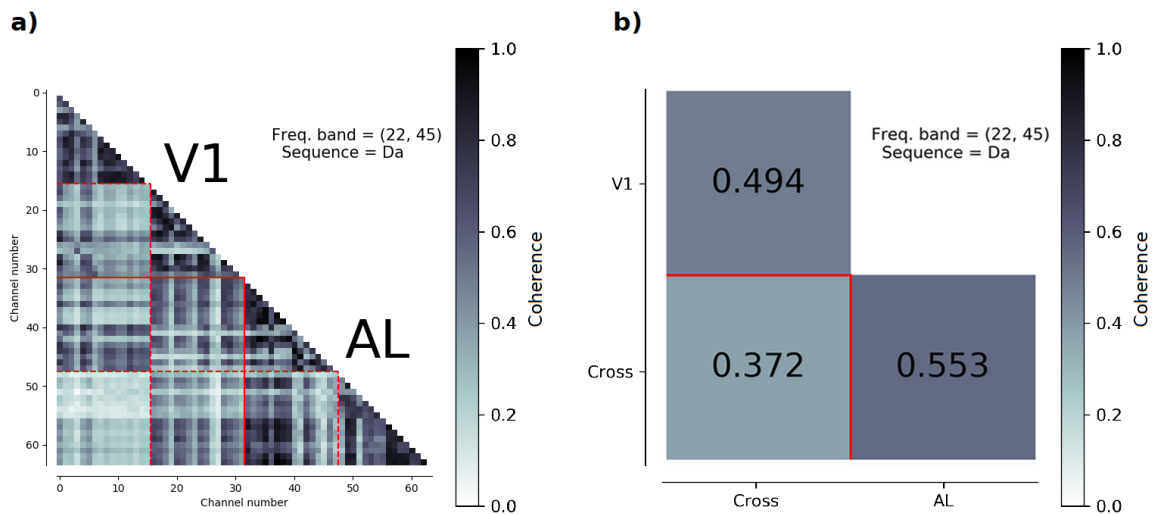


Figure 24. **Formulation of averaged measures.** a) Total coherency map between all the channels. Values have been averaged in the annotated frequency band (from 22 to 45 Hz) for every channel during stimulus A embedded in the D standard session (bimodal mismatch). b) Spatially averaged values. Averaging was done within the cortices (V1, AL) and between them (Cross).

the difference but also show the absolute value so that the relative size of the discrepancy

can be seen, too. Figure 25. shows an example how it looks like for our results. Colouring for the bars are stimulus-dependent and the grouping is based on the frequency bands. Hatching is created in order to visualise discrepancy better. These are the most meaningful figures and later, I will combine them into multiplots.

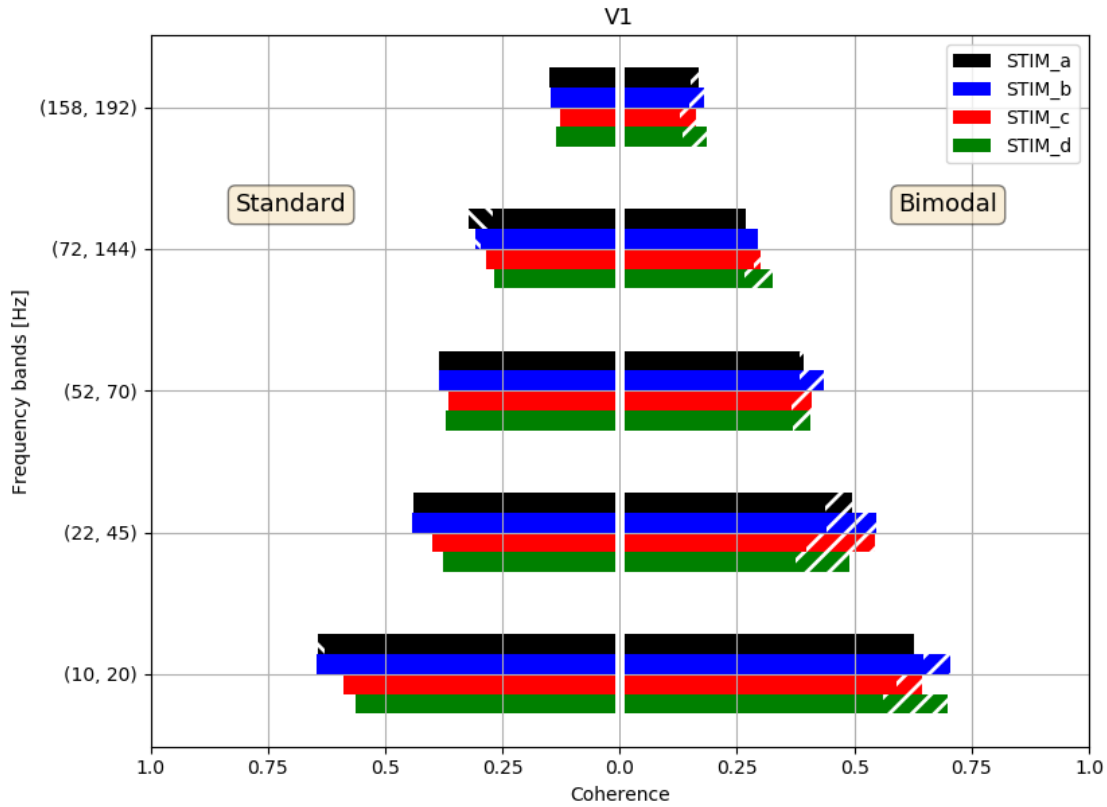


Figure 25. **Violinplot of the coherence of the bimodal traditional mismatch in the V1 cortex.** Different colours mean the stimuli, and hatching is also made to indicate discrepancy.

4.4.1 Mismatch comparisons

In this section, I am going to elaborate on all the results based on the mismatch comparisons. Each paragraph is going to tell about either an overall phenomena or a type of mismatch.

Decreasing coherence As fig. 23. also shows, coherence is inversely proportional to frequency. This is largely due to the pink noise. This artefact has a decreasing manner in terms of amplitude which also plays a crucial role in coherence also. To resolve this problem, I encourage the reader to focus on the differences. Furthermore, since pink

noise is present in all biological systems and is mostly independent of the stimulus, we can observe decline in coherence for every violinplot. However, this effect is smaller for cross-coherence plots since due to volume conduction (intervening tissue (skull, skin etc.) conducts charge) closely placed sensors can detect the same source.

Smaller cross-coherence Coherence between channels in different brain regions show smaller values and less affected by the noise. Furthermore, these plots are the result of averaging over $32 \times 32 = 1024$ comparisons as opposed to $\frac{32 \times 31}{2} = 496$ occasions. Remaining noise is decreased in this way further.

M-ISI at high frequencies Another common attribute of the plots is that bars for the M-ISI sequences have a higher coherence everywhere, regardless of the region. For stimulus specificity, stimulus D showed the highest of coherence in every region, which (along with the others) can be caused by the awakening of the animal.

Visual mismatches Figure 26. shows all the possible comparisons between the coherences between signals that create visual mismatches. Traditional comparisons do not show large differences, only the lower beta (10-20 Hz) frequencies have a higher, and stimulus specific direction. For stimulus C and D (vertically grating mismatches, the coherence increased). On the other hand, equiprobable sequences had higher value for higher frequency band, and for the AL cortex, a more moderate increase can be seen also without stimulus and frequency band. High values of M-ISI can be explained by the increase of excitability due to longer idle time.

Auditory mismatches The most obvious difference between the previous and 27. figure is the increase in discrepancy for the traditional mismatches. High beta and low gamma bands (22-45, 52-70, 72-144 Hz) show a decent amount of difference, which is remnant for the genuine mismatch also (equiprobable-deviant), i.e., auditory mismatch caused more activity since the animal was in an anaesthetised state. However, for lower frequency bands, M-ISI sessions did not produce greater, but for the others all the more so. An involvement of other brain regions can be an explanation.

Bimodal mismatches Bimodal mismatch present the highest activity in the 52-70 Hz band in the AL among other mismatches (fig. 28.). All the other differences show similar pattern to the traditional, genuine and M-ISI-type auditory mismatch. The fact that most of the larger differences were caused by auditory mismatch, in bimodal mismatches the visual part only slightly changes the outcoming results.

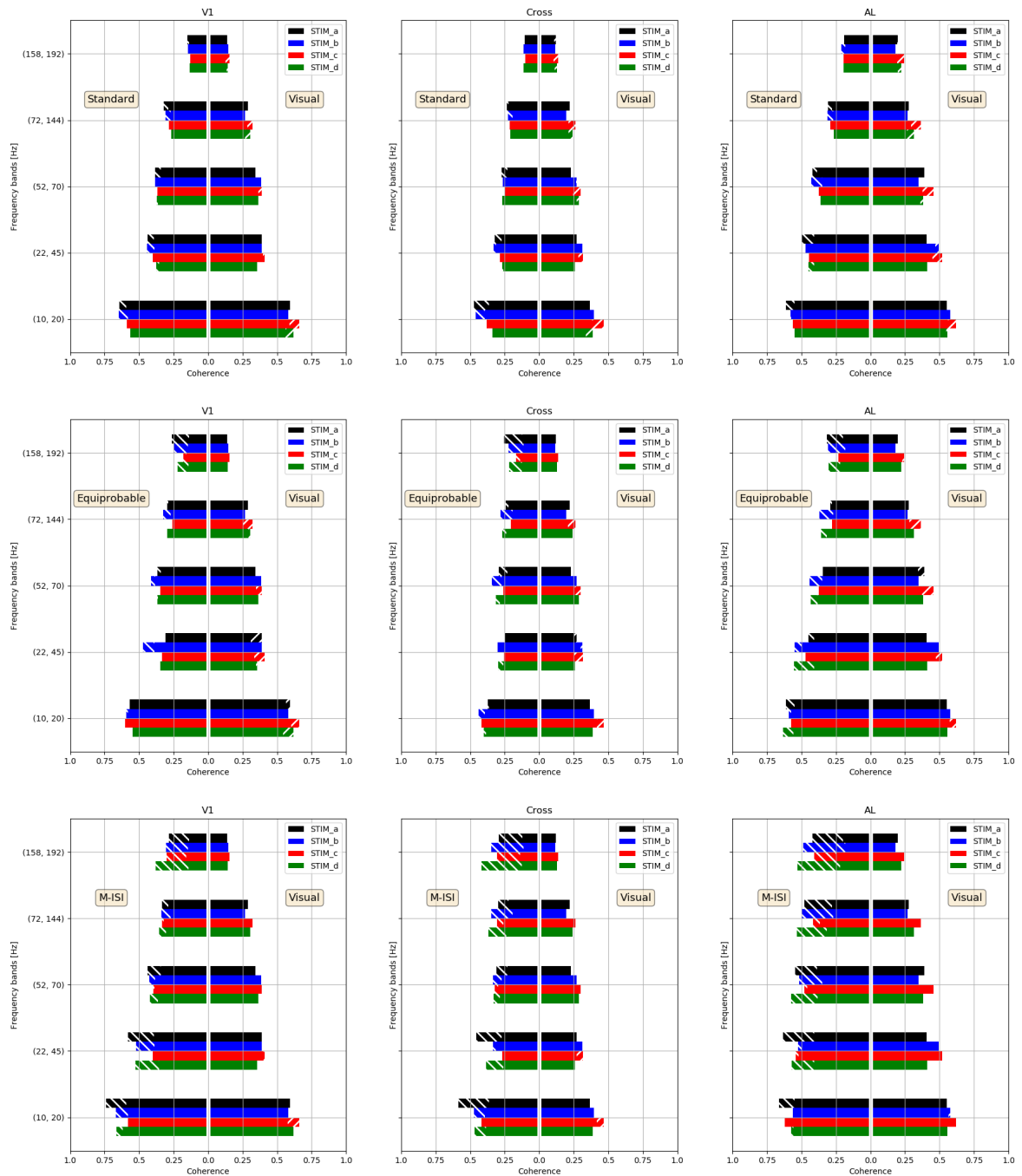


Figure 26. **Violinplots for the visual mismatches.** Columns refer to coherence by region and rows are for different mismatch methods. Colours denote different stimuli and hatches meant to indicate discrepancy.

4.4.2 Non-mismatch comparisons

Figure 29. shows those comparisons which not contained deviant signals. Except for the highest frequency band, random probability only slightly changed the values. However, now we can analyse how fatigue influenced the experiment; most of the times –in the same regions– activity appeared to decrease from stimulus A to D. For the highest frequency band (158-192 Hz) it is important to mention that high-frequency neural activity overlaps

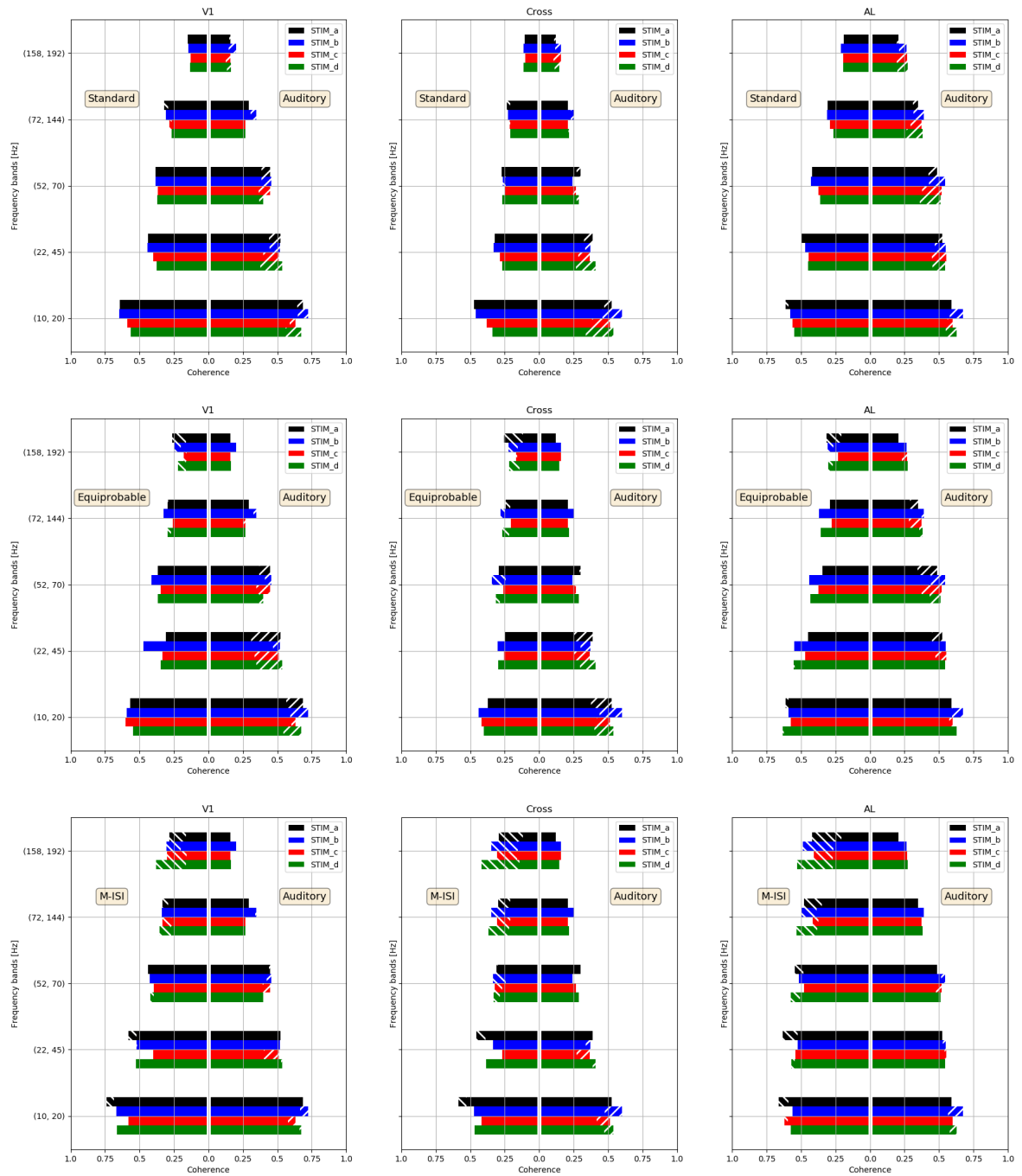


Figure 27. **Violinplots for the auditory mismatches.** Columns refer to coherence by region and rows are for different mismatch methods. Colours denote different stimuli and hatches meant to indicate discrepancy.

entirely with the spectral bandwidth of muscle activity ($\sim 20\text{--}300$ Hz) [71]. This applies for the M-ISI session also, since as the anaesthetic state of the animal changed movements of it could occur. Furthermore, lower bandwidths are not part of this and therefore here simply just the activity is what has risen. No stimulus specificity is visible.

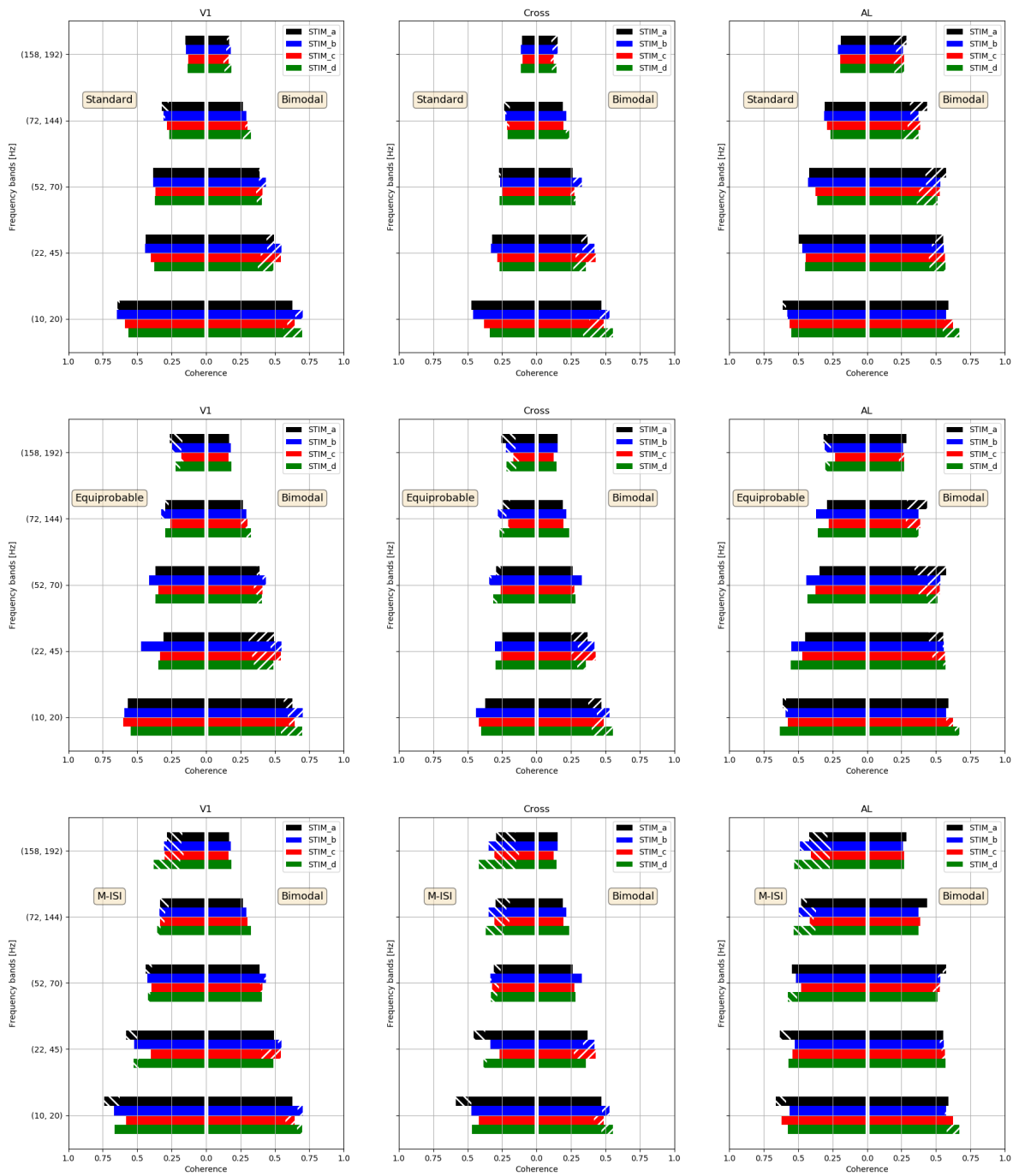


Figure 28. Violinplots for the bimodal mismatches. Columns refer to coherence by region and rows are for different mismatch methods. Colours denote different stimuli and hatches meant to indicate discrepancy.

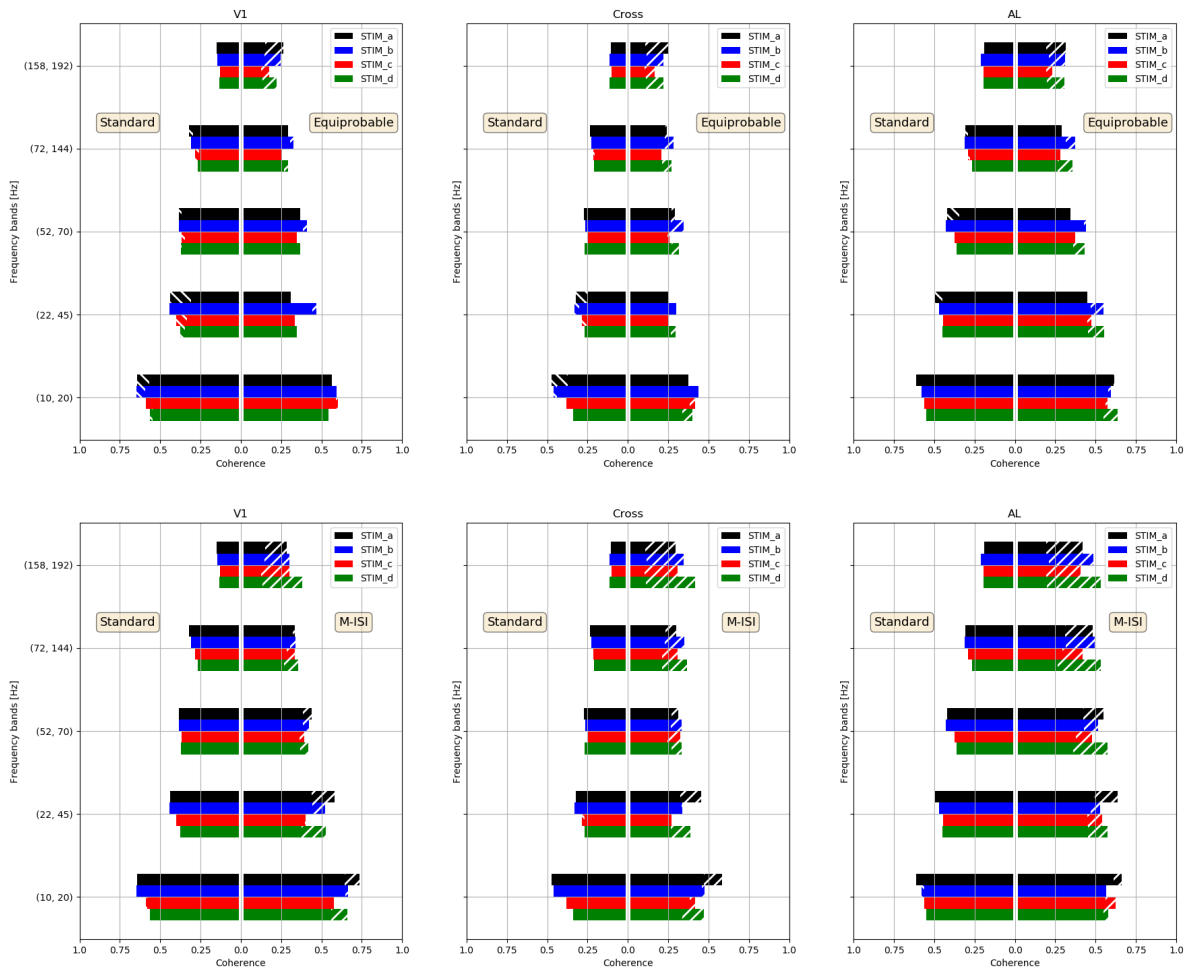


Figure 29. **Violinplots for the non-mismatch comparisons.** Columns refer to coherence by region and rows are for different combinations. Colours denote different stimuli and hatches meant to indicate discrepancy.

5 Discussion

My main goal to create measures that give meaningful results is achieved. These four types of methods allow us to analyse different aspects of the same data and draw conclusions. We included statistical hypothesis testing and gave phenomenological insights to govern our evaluation. Each method highlighted different aspects of the results which will be useful in the future for to run on different animals. In this section I am going to review all the deductions we made and see whether they agree with the literature.

Temporal evaluation Zeroth step of all. Indication of either stimulus specific adaptation or fatigue during later standard sessions (stimuli C and D) appeared. Cortical activity in terms of device depth has also been revealed and separated different areas based on activity. We also noticed that channels that show high activity tend to depend on the mismatch method and deduced that fatigue with the change of the anaesthetic state has a crucial effect. Furthermore, results suggested that the change of inter-stimulus interval had a higher impact on activity than deviance detection.

Spiking activity Dominant cells have been identified on channels and grouped together based on temporal activity. Stimulus-specific adaptation/fatigue appeared here also. More cells and therefore activity could be detected from the V1 cortex than from the AL. Both excitatory and inhibitory cells were found.

Frequency map Using the codes for comparisons made it easier to notice the main, non-novel types of auditory, visual, and bimodal MMNs (with their strength for stimulus types) and the possible emergence of conditional mismatch negativity. Both visual and auditory mismatch have shown stimulus specificity by regions and genuine bimodal mismatch negativity has indirectly proven the existence of SSA. Furthermore, these results emphasised the importance of different bands in brainwaves and directed our attention towards coherence.

Coherence Coherence was more or less in accordance with the results we got from the frequency map and did serve us new knowledge about the difference in information propagation between cortical regions. For non-mismatch comparison we did see that how the modification of ISI influences to excitability. Nevertheless, the anaesthetic state of the animal did play a crucial role here as the M-ISI sequences has shown a greater coherence for high frequency components.

Changes in beta and gamma frequency bands have been linked to attention and expectation in human auditory cortex for auditory stimuli [72]. Furthermore, another study conducted on humans has demonstrated a gamma-to-beta transition to novel

auditory stimuli, and correlations between beta and gamma bands had shown high interdependence [73]. Our results are in accordance with these articles: we found differences in the same frequency regions for bimodal stimulation based on the results of frequency maps and coherence in two regions of a mouse. To verify our observations, we are preparing to run the evaluations on other mice also with different electrode placements.

Not every aspect of the data has been analysed as well as not every method has been mentioned in this thesis either. We also tried cluster-analysing on the cells, correlation between firing frequency of cells and power spectrum, machine learning on frequency components, etc. These were the ones which would form a whole, coherent set of methods to use on other animals. Nevertheless, modification of parameters such as frequency bands, averaged areas or even the measure itself (coherency, imaginary coherence or phase-locking value) could have given different results. Results have been presented in an understandable way despite the myriad of possible approaches on the data.

Our next and final step is going to be to run these analysis methods on the other animals with respect to different recording sites, task order and notes on animal. After all those we will be able to draw conclusions in biological sense also which will either confirm or disprove our theories on multimodal signal processing. Lastly, publication is planned to be submitted by the end of the year.

6 References

- [1] Herculano-Houzel, S. (2009). The human brain in numbers: a linearly scaled-up primate brain. *Frontiers in Human Neuroscience*, 3, 31. <https://doi.org/10.3389/neuro.09.031.2009>
- [2] Hall, John (2011). *Guyton and Hall Textbook of Medical Physiology* (12th ed.). Philadelphia, PA: Saunders/Elsevier. ISBN 978-1-4160-4574-8.
- [3] Rutecki PA (April 1992). "Neuronal excitability: voltage-dependent currents and synaptic transmission". *Journal of Clinical Neurophysiology*. 9 (2): 195–211. doi:10.1097/00004691-199204010-00003. PMID 1375602.
- [4] Thanapitak, Surachoke. (2012). *Bionics Chemical Synapse*. 10.13140/RG.2.1.2295.1288.
- [5] Rugg, M. D., Coles, M. G. H., Coles, M. G. H., Rugg, M. D. (2008). Event-related brain potentials: an introduction. In *Electrophysiology of Mind*. <https://doi.org/10.1093/acprof:oso/9780198524168.003.0001>

- [6] Pérez-González, D., Malmierca, M. S. (2014). Adaptation in the auditory system: An overview. *Frontiers in Integrative Neuroscience*. <https://doi.org/10.3389/fnint.2014.00019>
- [7] Folstein, J. R., Van Petten, C. (2008). Influence of cognitive control and mismatch on the N2 component of the ERP: A review. *Psychophysiology*. <https://doi.org/10.1111/j.1469-8986.2007.00602.x>
- [8] Polich, J. (2007). Updating P300: An integrative theory of P3a and P3b. *Clinical Neurophysiology*. <https://doi.org/10.1016/j.clinph.2007.04.019>
- [9] Näätänen R, Paavilainen P, Tiitinen H, Jiang D, Alho K. Attention and mismatch negativity. *Psychophysiology*. 1993;30(5):436–450. doi:10.1111/j.1469-8986.1993.tb02067.x
- [10] Näätänen, R. (1992). *Attention and brain function*. Lawrence Erlbaum Associates, Inc.
- [11] Brattico E, Tervaniemi M, Näätänen R, Peretz I (October 2006). "Musical scale properties are automatically processed in the human auditory cortex" (PDF). *Brain Research*. 1117 (1): 162–74. doi:10.1016/j.brainres.2006.08.023. PMID 16963000.
- [12] Astikainen, P., Ruusuvirta, T., Wikgren, J., Korhonen, T. (2004). The human brain processes visual changes that are not cued by attended auditory stimulation. *Neuroscience Letters*, 368(2), 231–234.
- [13] Czigler, I., Balázs, L., Pató, L. G. (2004). Visual change detection: event-related potentials are dependent on stimulus location in humans. *Neuroscience Letters*, 364(3), 149–153.
- [14] Pazo-Alvarez, P., Cadaveira, F., Amenedo, E. (2003). MMN in the visual modality: a review. *Biological Psychology*, 63(3), 199–236.
- [15] Kekoni, J., Hämäläinen, H., Saarinen, M., Gröhn, J., Reinikainen, K., Lehtokoski, A., Näätänen, R. (1997). Rate effect and mismatch responses in the somatosensory system: ERP-recordings in humans. *Biological Psychology*, 46(2), 125–142.
- [16] NÄÄTÄNEN, R. (2001). The perception of speech sounds by the human brain as reflected by the mismatch negativity (MMN) and its magnetic equivalent (MMNm). *Psychophysiology*, 38(1), 1–21. <https://doi.org/10.1111/1469-8986.3810001>
- [17] Baldeweg, T., Richardson, A., Watkins, S., Foale, C., Gruzelier, J. (1999). Impaired auditory frequency discrimination in dyslexia detected with mismatch evoked potentials. *Annals of Neurology: Official Journal of the American Neurological Association and the Child Neurology Society*, 45(4), 495–503.

- [18] Iyer, P. M., Mohr, K., Broderick, M., Gavin, B., Burke, T., Bede, P., ... Nasseroleslami, B. (2017). Mismatch Negativity as an Indicator of Cognitive Sub-Domain Dysfunction in Amyotrophic Lateral Sclerosis. *Frontiers in Neurology*, 8, 395. <https://doi.org/10.3389/fneur.2017.00395>
- [19] Opitz, B., Rinne, T., Mecklinger, A., Von Cramon, D. Y., Schröger, E. (2002). Differential contribution of frontal and temporal cortices to auditory change detection: FMRI and ERP results. *NeuroImage*. <https://doi.org/10.1006/nimg.2001.0970>
- [20] Rinne, T., Alho, K., Ilmoniemi, R. J., Virtanen, J., Näätänen, R. (2000). Separate time behaviors of the temporal and frontal mismatch negativity sources. *NeuroImage*. <https://doi.org/10.1006/nimg.2000.0591>
- [21] Doeller, C. F., Opitz, B., Mecklinger, A., Krick, C., Reith, W., Schröger, E. (2003). Prefrontal cortex involvement in preattentive auditory deviance detection: Neuroimaging and electrophysiological evidence. *NeuroImage*. [https://doi.org/10.1016/S1053-8119\(03\)00389-6](https://doi.org/10.1016/S1053-8119(03)00389-6)
- [22] Giard, M. -H, Perrin, F., Pernier, J., Bouchet, P. (1990). Brain Generators Implicated in the Processing of Auditory Stimulus Deviance: A Topographic Event-Related Potential Study. *Psychophysiology*. <https://doi.org/10.1111/j.1469-8986.1990.tb03184.x>
- [23] Garrido, M. I., Kilner, J. M., Stephan, K. E., Friston, K. J. (2009). The mismatch negativity: a review of underlying mechanisms. *Clinical Neurophysiology*, 120(3), 453–463.
- [24] Näätänen, R., Pakarinen, S., Rinne, T., Takegata, R. (2004). The mismatch negativity (MMN): Towards the optimal paradigm. *Clinical Neurophysiology*. <https://doi.org/10.1016/j.clinph.2003.04.001>
- [25] Tervaniemi, M., Ilvonen, T., Sinkkonen, J., Kujala, A., Alho, K., Huotilainen, M., Näätänen, R. (2000). Harmonic partials facilitate pitch discrimination in humans: Electrophysiological and behavioral evidence. *Neuroscience Letters*. [https://doi.org/10.1016/S0304-3940\(99\)00941-6](https://doi.org/10.1016/S0304-3940(99)00941-6)
- [26] Bottcher-Gandor, C., Ullsperger, P. (1992). Mismatch Negativity in Event-Related Potentials to Auditory Stimuli as a Function of Varying Interstimulus Interval. *Psychophysiology*. <https://doi.org/10.1111/j.1469-8986.1992.tb02028.x>
- [27] Kane, N. M., Curry, S. H., Butler, S. R., Cummins, B. H. (1993). Electrophysiological indicator of awakening from coma. *The Lancet*. [https://doi.org/10.1016/0140-6736\(93\)90453-N](https://doi.org/10.1016/0140-6736(93)90453-N)
- [28] Kujala, T., Tervaniemi, M., Schröger, E. (2007). The mismatch negativity in cognitive and clinical neuroscience: Theoretical and methodological considerations. *Biological Psychology*. <https://doi.org/10.1016/j.biopsycho.2006.06.001>

- [29] Näätänen, R. (2000). Mismatch negativity (MMN): Perspectives for application. *International Journal of Psychophysiology*. [https://doi.org/10.1016/S0167-8760\(00\)00091-X](https://doi.org/10.1016/S0167-8760(00)00091-X)
- [30] Escera, C., Alho, K., Winkler, I., Näätänen, R. (1998). Neural mechanisms of involuntary attention to acoustic novelty and change. *Journal of Cognitive Neuroscience*. <https://doi.org/10.1162/089892998562997>
- [31] Oranje, B., Van Berckel, B. N. M., Kemner, C., Van Ree, J. M., Kahn, R. S., Verbaten, M. N. (2000). The effects of a sub-anaesthetic dose of ketamine on human selective attention. *Neuropsychopharmacology*. [https://doi.org/10.1016/S0893-133X\(99\)00118-9](https://doi.org/10.1016/S0893-133X(99)00118-9)
- [32] Tiitinen, H., May, P., Reinikainen, K., Näätänen, R. (1994). Attentive novelty detection in humans is governed by pre-attentive sensory memory. *Nature*. <https://doi.org/10.1038/372090a0>
- [33] Winkler, I., Karmos, G., Näätänen, R. (1996). Adaptive modeling of the unattended acoustic environment reflected in the mismatch negativity event-related potential. *Brain Research*. [https://doi.org/10.1016/S0006-8993\(96\)01008-6](https://doi.org/10.1016/S0006-8993(96)01008-6)
- [34] Näätänen, R., Winkler, I. (1999). The concept of auditory stimulus representation in cognitive neuroscience. *Psychological Bulletin*. <https://doi.org/10.1037/0033-2909.125.6.826>
- [35] Sussman, E., Winkler, I. (2001). Dynamic sensory updating in the auditory system. *Cognitive Brain Research*. [https://doi.org/10.1016/S0926-6410\(01\)00067-2](https://doi.org/10.1016/S0926-6410(01)00067-2)
- [36] Alain, C., Woods, D. L., Knight, R. T. (1998). A distributed cortical network for auditory sensory memory in humans. *Brain Research*. [https://doi.org/10.1016/S0006-8993\(98\)00851-8](https://doi.org/10.1016/S0006-8993(98)00851-8)
- [37] Romanski, L. M., Tian, B., Fritz, J., Mishkin, M., Goldman-Rakic, P. S., Rauschecker, J. P. (1999). Dual streams of auditory afferents target multiple domains in the primate prefrontal cortex. *Nature Neuroscience*. <https://doi.org/10.1038/16056>
- [38] Jääskeläinen, I. P., Ahveninen, J., Bonmassar, G., Dale, A. M., Ilmoniemi, R. J., Levänen, S., ... Belliveau, J. W. (2004). Human posterior auditory cortex gates novel sounds to consciousness. *Proceedings of the National Academy of Sciences of the United States of America*. <https://doi.org/10.1073/pnas.0303760101>
- [39] Winkler, I., Tervaniemi, M., Näätänen, R. (1997). Two separate codes for missing-fundamental pitch in the human auditory cortex. *The Journal of the Acoustical Society of America*. <https://doi.org/10.1121/1.419860>

- [40] Atienza, M., Cantero, J. L. (2001). Complex sound processing during human REM sleep by recovering information from long-term memory as revealed by the mismatch negativity (MMN). *Brain Research*. [https://doi.org/10.1016/S0006-8993\(01\)02340-X](https://doi.org/10.1016/S0006-8993(01)02340-X)
- [41] Näätänen, R., Paavilainen, P., Alho, K., Reinikainen, K., Sams, M. (1989). Do event-related potentials reveal the mechanism of the auditory sensory memory in the human brain? *Neuroscience Letters*. [https://doi.org/10.1016/0304-3940\(89\)90513-2](https://doi.org/10.1016/0304-3940(89)90513-2)
- [42] Hari, R., Rif, J., Tiihonen, J., Sams, M. (1992). Neuromagnetic mismatch fields to single and paired tones. *Electroencephalography and Clinical Neurophysiology*. [https://doi.org/10.1016/0013-4694\(92\)90159-F](https://doi.org/10.1016/0013-4694(92)90159-F)
- [43] TIITINEN, H., ALHO, K., HUOTILAINEN, M., ILMONIEMI, R. J., SIMOLA, J., NÄÄTÄNEN, R. (1993). Tonotopic auditory cortex and the magnetoencephalographic (MEG) equivalent of the mismatch negativity. *Psychophysiology*. <https://doi.org/10.1111/j.1469-8986.1993.tb02078.x>
- [44] Friston, K. (2003). Learning and inference in the brain. *Neural Networks*. <https://doi.org/10.1016/j.neunet.2003.06.005>
- [45] Friston, K. (2005). A theory of cortical responses. *Philosophical Transactions of the Royal Society B: Biological Sciences*. <https://doi.org/10.1098/rstb.2005.1622>
- [46] Baldeweg, T., Wong, D., Stephan, K. E. (2006). Nicotinic modulation of human auditory sensory memory: Evidence from mismatch negativity potentials. *International Journal of Psychophysiology*. <https://doi.org/10.1016/j.ijpsycho.2005.07.014>
- [47] Rao, R. P. N., Ballard, D. H. (1999). Predictive coding in the visual cortex: A functional interpretation of some extra-classical receptive-field effects. *Nature Neuroscience*. <https://doi.org/10.1038/4580>
- [48] Yuille, A., Kersten, D. (2006). Vision as Bayesian inference: analysis by synthesis? *Trends in Cognitive Sciences*. <https://doi.org/10.1016/j.tics.2006.05.002>
- [49] Mumford, D. (1991). On the computational architecture of the neocortex. *Biological Cybernetics*. <https://doi.org/10.1007/bf00202389>
- [50] Taaseh, N., Yaron, A., Nelken, I. (2011). Stimulus-specific adaptation and deviance detection in the rat auditory cortex. *PLoS ONE*. <https://doi.org/10.1371/journal.pone.0023369>
- [51] Sams, M., Hämäläinen, M., Antervo, A., Kaukoranta, E., Reinikainen, K., Hari, R. (1985). Cerebral neuromagnetic responses evoked by short auditory stimuli. *Electroencephalography and Clinical Neurophysiology*. [https://doi.org/10.1016/0013-4694\(85\)91092-2](https://doi.org/10.1016/0013-4694(85)91092-2)

- [52] Jacobsen, T., Schröger, E. (2001). Is there pre-attentive memory-based comparison of pitch? *Psychophysiology*. <https://doi.org/10.1017/S0048577201000993>
- [53] Jacobsen, T., Schröger, E., Horenkamp, T., Winkler, I. (2003). Mismatch negativity to pitch change: Varied stimulus proportions in controlling effects of neural refractoriness on human auditory event-related brain potentials. *Neuroscience Letters*. [https://doi.org/10.1016/S0304-3940\(03\)00408-7](https://doi.org/10.1016/S0304-3940(03)00408-7)
- [54] Farley, B. J., Quirk, M. C., Doherty, J. J., Christian, E. P. (2010). Stimulus-specific adaptation in auditory cortex is an NMDA-independent process distinct from the sensory novelty encoded by the mismatch negativity. *Journal of Neuroscience*. <https://doi.org/10.1523/JNEUROSCI.2793-10.2010>
- [55] Fishman, Y. I., Steinschneider, M. (2012). Searching for the mismatch negativity in primary auditory cortex of the awake monkey: Deviance detection or stimulus specific adaptation? *Journal of Neuroscience*. <https://doi.org/10.1523/JNEUROSCI.2835-12.2012>
- [56] Grimm, S., Escera, C. (2012). Auditory deviance detection revisited: Evidence for a hierarchical novelty system. *International Journal of Psychophysiology*. <https://doi.org/10.1016/j.ijpsycho.2011.05.012>
- [57] Kimura, M., Katayama, J., Ohira, H., Schröger, E. (2009). Visual mismatch negativity: New evidence from the equiprobable paradigm. *Psychophysiology*. <https://doi.org/10.1111/j.1469-8986.2008.00767.x>
- [58] Astikainen, P., Lillstrang, E., Ruusuvirta, T. (2008). Visual mismatch negativity for changes in orientation - A sensory memory-dependent response. *European Journal of Neuroscience*. <https://doi.org/10.1111/j.1460-9568.2008.06510.x>
- [59] Czigler, I., Balázs, L., Winkler, I. (2002). Memory-based detection of task-irrelevant visual changes. *Psychophysiology*. <https://doi.org/10.1111/1469-8986.3960869>
- [60] Astikainen, P., Cong, F., Ristaniemi, T., Hietanen, J. K. (2013). Event-related potentials to unattended changes in facial expressions: Detection of regularity violations or encoding of emotions? *Frontiers in Human Neuroscience*. <https://doi.org/10.3389/fnhum.2013.00557>
- [61] Li, X., Lu, Y., Sun, G., Gao, L., Zhao, L. (2012). Visual mismatch negativity elicited by facial expressions: New evidence from the equiprobable paradigm. *Behavioral and Brain Functions*. <https://doi.org/10.1186/1744-9081-8-7>
- [62] Kaliukhovich, D. A., Vogels, R. (2014). Neurons in macaque inferior temporal cortex show no surprise response to deviants in visual oddball sequences. *Journal of Neuroscience*. <https://doi.org/10.1523/JNEUROSCI.2154-14.2014>

- [63] Amado, C., Kovács, G. (2016). Does surprise enhancement or repetition suppression explain visual mismatch negativity? *European Journal of Neuroscience*. <https://doi.org/10.1111/ejn.13263>
- [64] Okuyama, T. (2018). Social memory engram in the hippocampus. *Neuroscience Research*. <https://doi.org/10.1016/j.neures.2017.05.007>
- [65] Shin, K, Hammond, J. *Fundamentals of signal processing for sound and vibration engineers*. John Wiley and Sons, 2008.
- [66] Gramfort, A., Luessi, M., Larson, E., Engemann, D. A., Strohmeier, D., Brodbeck, C., ... Hämäläinen, M. (2013). MEG and EEG data analysis with MNE-Python. *Frontiers in Neuroscience*. <https://doi.org/10.3389/fnins.2013.00267>
- [67] Dunn, O. J. (1958). Estimation of the Means of Dependent Variables. *The Annals of Mathematical Statistics*. <https://doi.org/10.1214/aoms/1177706443>
- [68] Wang, B., Ke, W., Guang, J., Chen, G., Yin, L., Deng, S., Shu, Y. (2016). Firing frequency maxima of fast-spiking neurons in human, monkey, and mouse neocortex. *Frontiers in Cellular Neuroscience*. <https://doi.org/10.3389/fncel.2016.00239>
- [69] Szendro, P., Vincze, G., Szasz, A. (2001). Bio-response to white noise excitation. *Electro- and Magnetobiology*. <https://doi.org/10.1081/JBC-100104145>
- [70] Besle, J., Caclin, A., Mayet, R., Delpuech, C., Lecaigard, F., Giard, M. H., Morlet, D. (2007). Audiovisual events in sensory memory. *Journal of Psychophysiology*. <https://doi.org/10.1027/0269-8803.21.34.231>
- [71] Muthukumaraswamy, S. D. (2013). High-frequency brain activity and muscle artifacts in MEG/EEG: A review and recommendations. *Frontiers in Human Neuroscience*. <https://doi.org/10.3389/fnhum.2013.00138>
- [72] Todorovic, A., Schoffelen, J. M., Van Ede, F., Maris, E., De Lange, F. P. (2015). Temporal expectation and attention jointly modulate auditory oscillatory activity in the beta band. *PLoS ONE*. <https://doi.org/10.1371/journal.pone.0120288>
- [73] Haenschel, C., Baldeweg, T., Croft, R. J., Whittington, M., Gruzelier, J. (2000). Gamma and beta frequency oscillations in response to novel auditory stimuli: A comparison of human electroencephalogram (EEG) data with in vitro models. *Proceedings of the National Academy of Sciences of the United States of America*. <https://doi.org/10.1073/pnas.120162397>

Appendices

A Temporal evaluation

All the results for the temporal evaluation are shown here.

A.1 Primary visual cortex (V1)

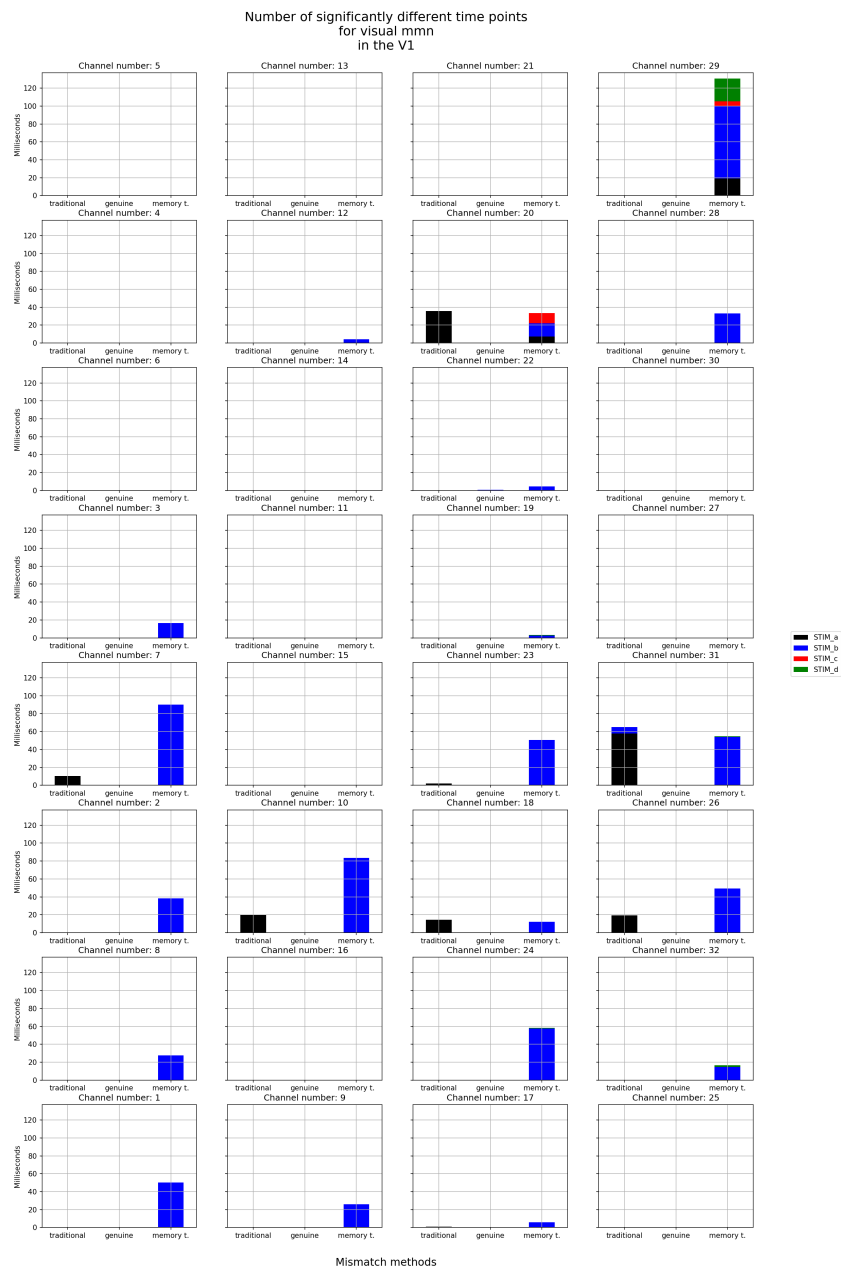


Figure 30. The length of significant differences for the visual mmn in the primary visual cortex (V1). Different stimulus types are noted with different colours and the stacked bars mean the mismatch methods. Level of significance was the Bonferroni corrected value of $\alpha = 0.05$.

Number of significantly different time points
for bimodal mmn
in the V1

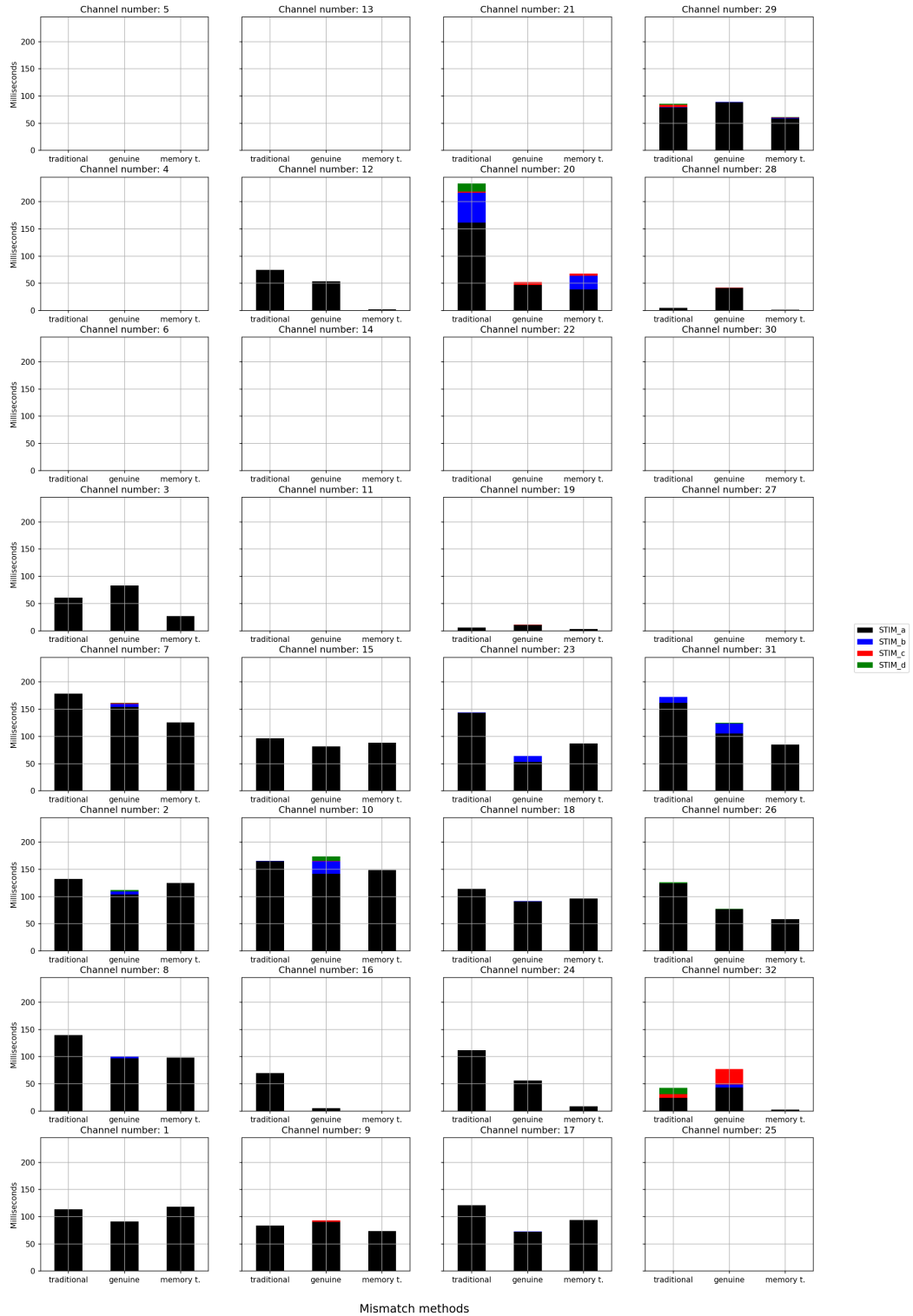


Figure 31. The length of significant differences for the bimodal mmn in the primary visual cortex (V1).

Number of significantly different time points
for non-mmn's
in the V1

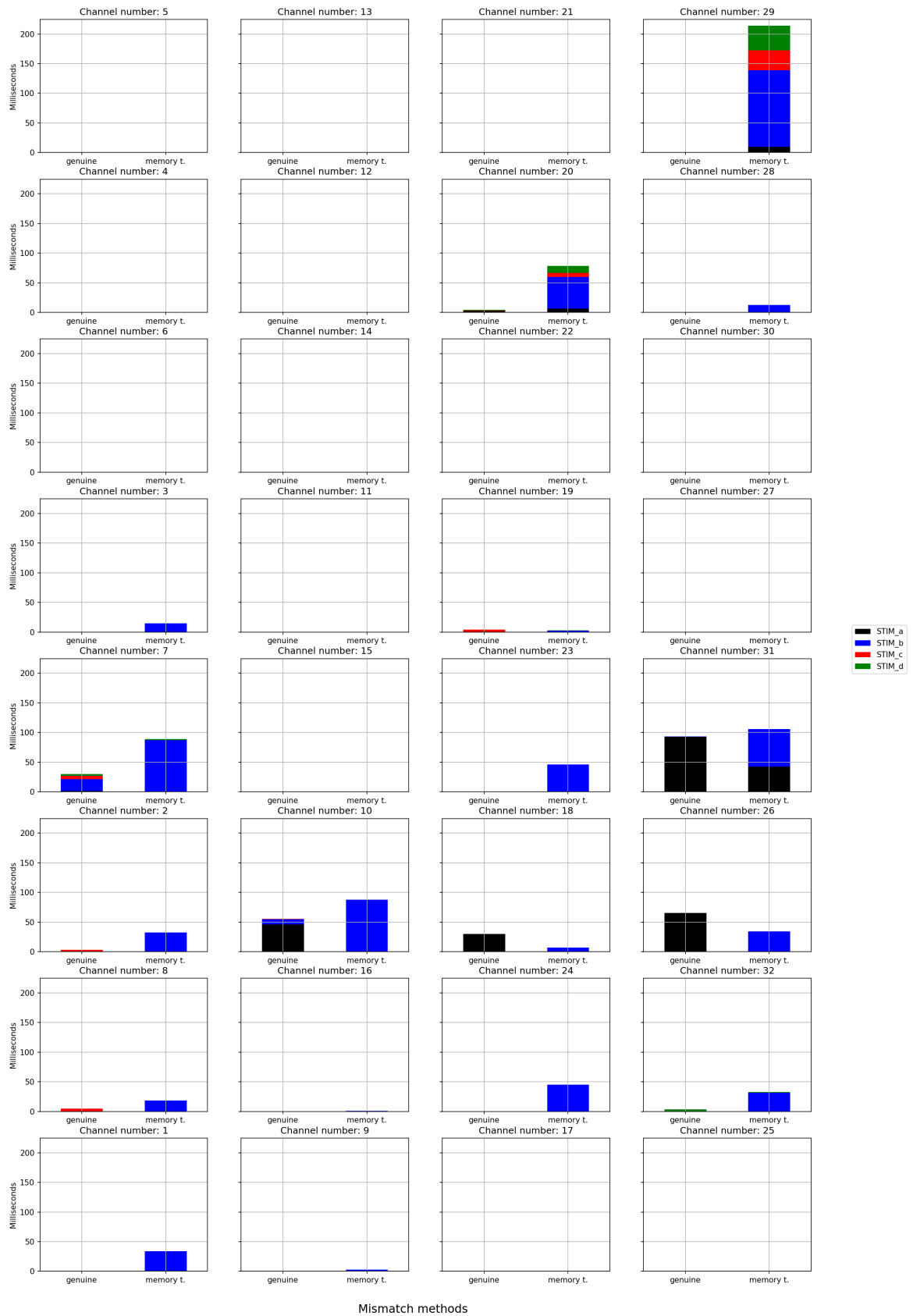


Figure 32. The length of significant differences for the non-mismatch comparisons in the primary visual cortex (V1). Different stimulus types are noted with different colours and the stacked bars mean the mismatch methods. Level of significance was the Bonferroni corrected value of $\alpha = 0.05$.

A.2 Anterolateral cortex (AL)



Figure 33. The length of significant differences for the auditory mmn in the anterolateral cortex (AL). Different stimulus types are noted with different colours and the stacked bars mean the mismatch methods. Level of significance was the Bonferroni corrected value of $\alpha = 0.05$.

Number of significantly different time points
for visual mmn
in the AL

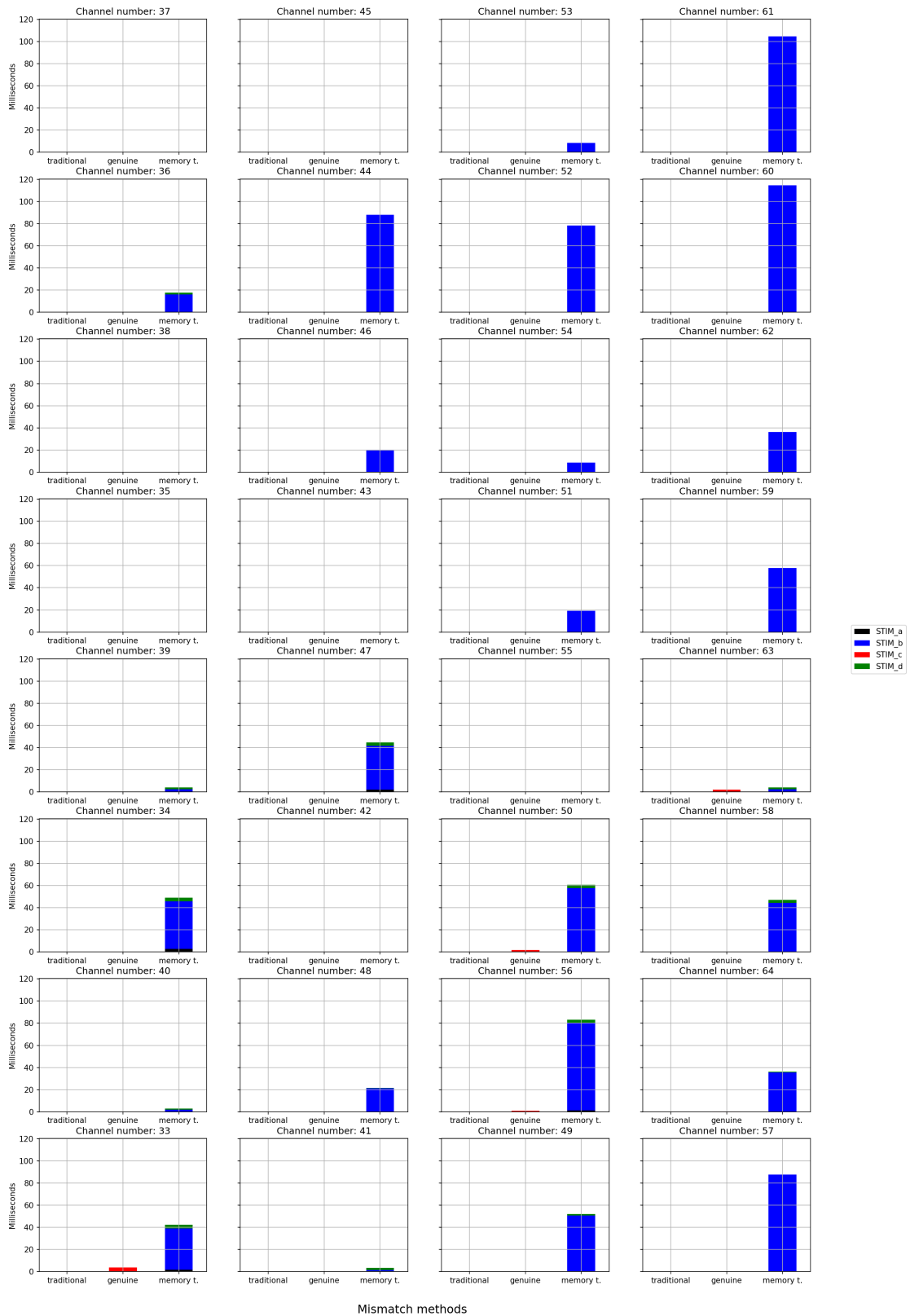


Figure 34. The length of significant differences for the visual mmn in the anterolateral cortex (AL). Different stimulus types are noted with different colours and the stacked bars mean the mismatch methods. Level of significance was the Bonferroni corrected value of $\alpha = 0.05$.

Number of significantly different time points
for bimodal mmn
in the AL

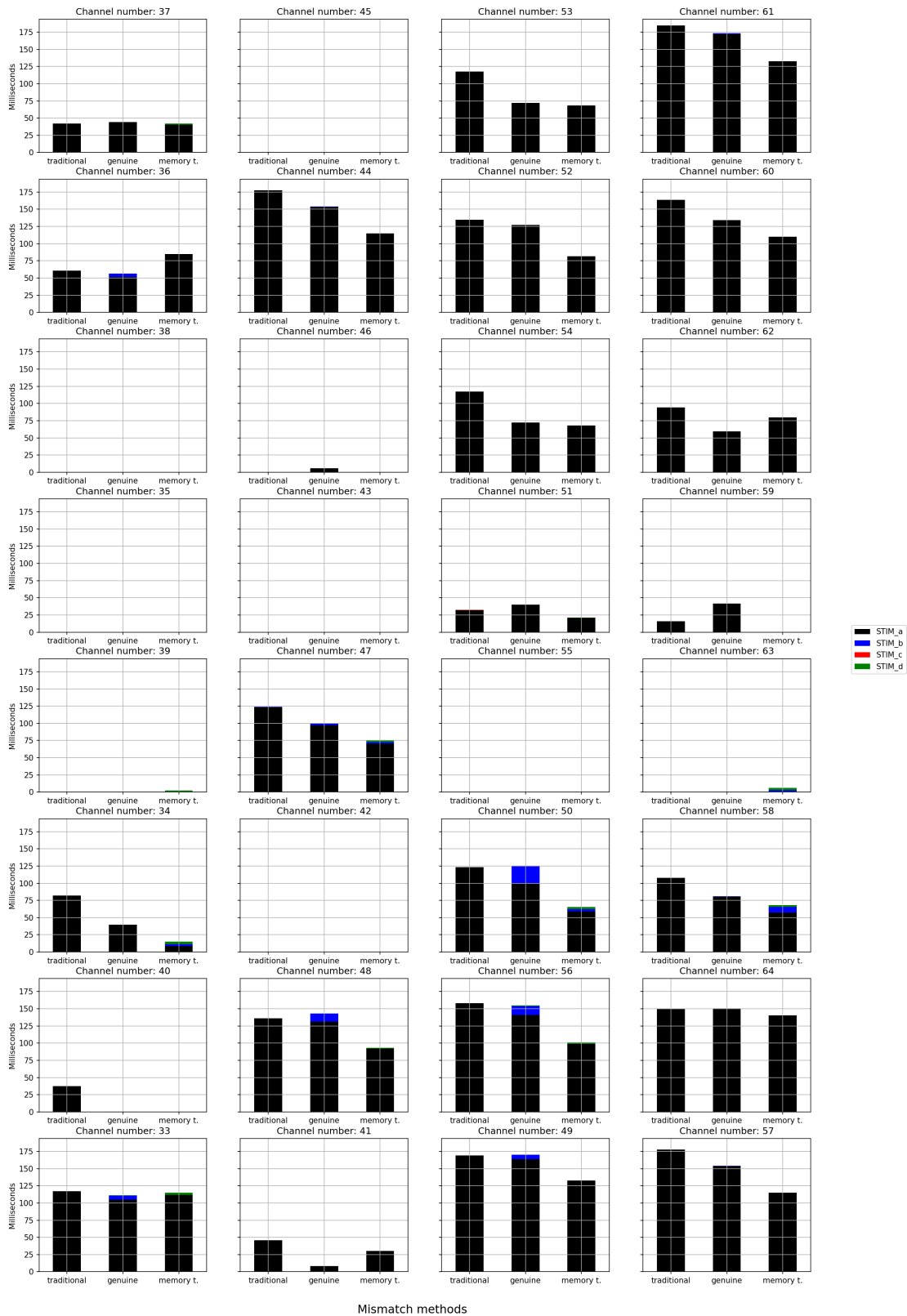


Figure 35. The length of significant differences for the bimodal mmn in the anterolateral cortex (AL). Different stimulus types are noted with different colours and the stacked bars mean the mismatch methods. Level of significance was the Bonferroni corrected value of $\alpha = 0.05$.

Number of significantly different time points
for non-mmn's
in the AL

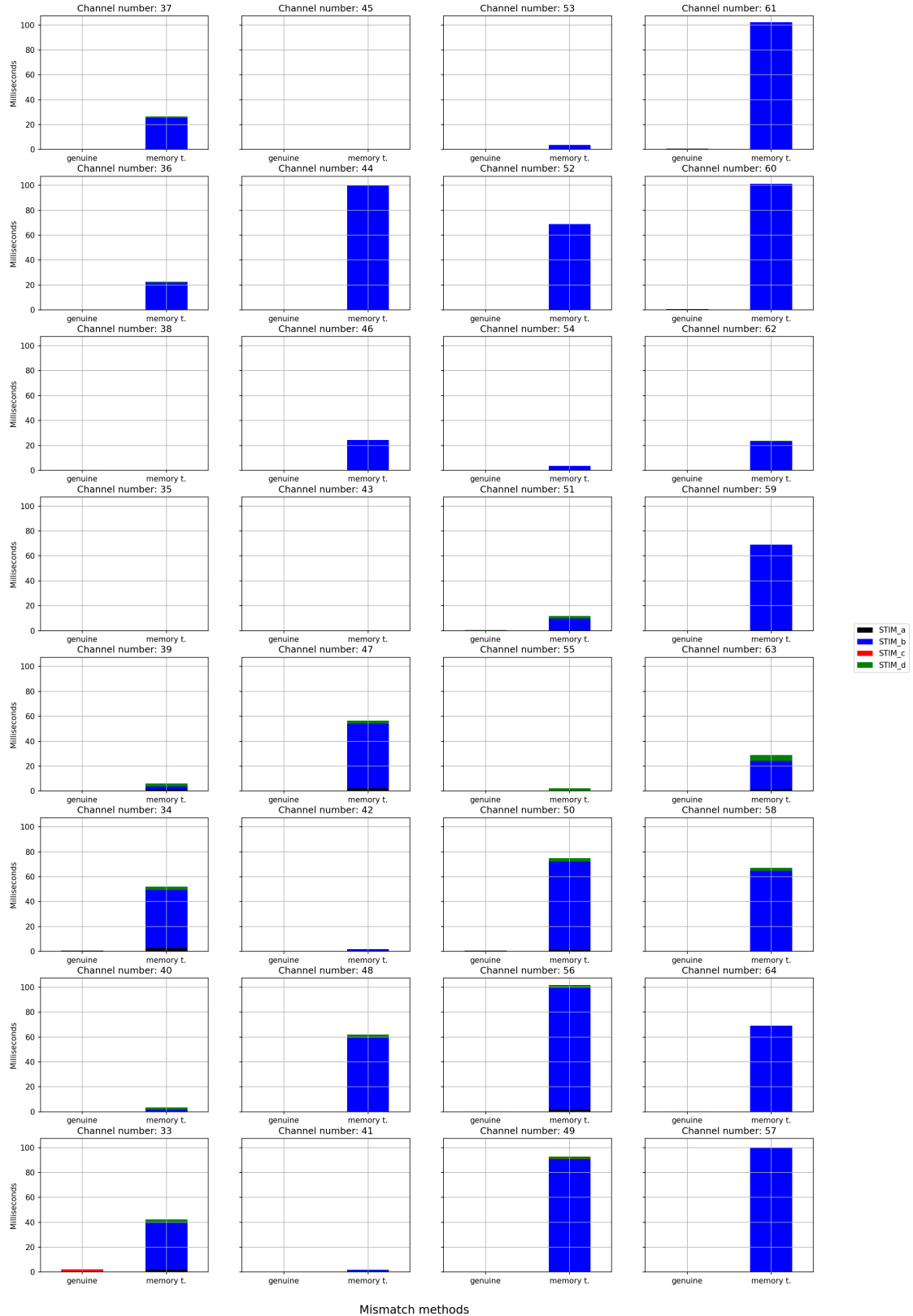


Figure 36. The length of significant differences for the non-mismatch comparisons in the anterolateral cortex (AL). Different stimulus types are noted with different colours and the stacked bars mean the mismatch methods. Level of significance was the Bonferroni corrected value of $\alpha = 0.05$.

B Spiking histograms

Supplementary results are found in this section.

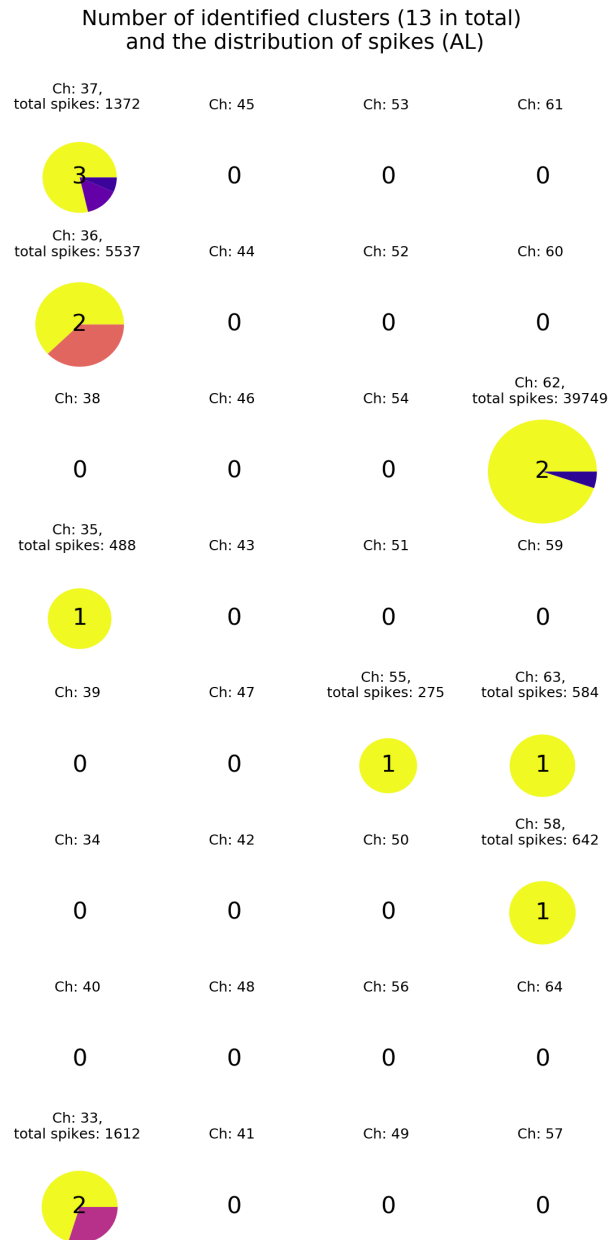


Figure 37. **Number of identified cells on one channel and the overall spiking activity at the anterolateral cortex (AL).** Radii of pie charts are calculated by dividing the natural logarithm of total number of spikes detected on a given channel by ten (for scaling). Colouring of these objects are based on the number of spikes for one neuron.

Average spiking frequency for the most active clusters (AL)

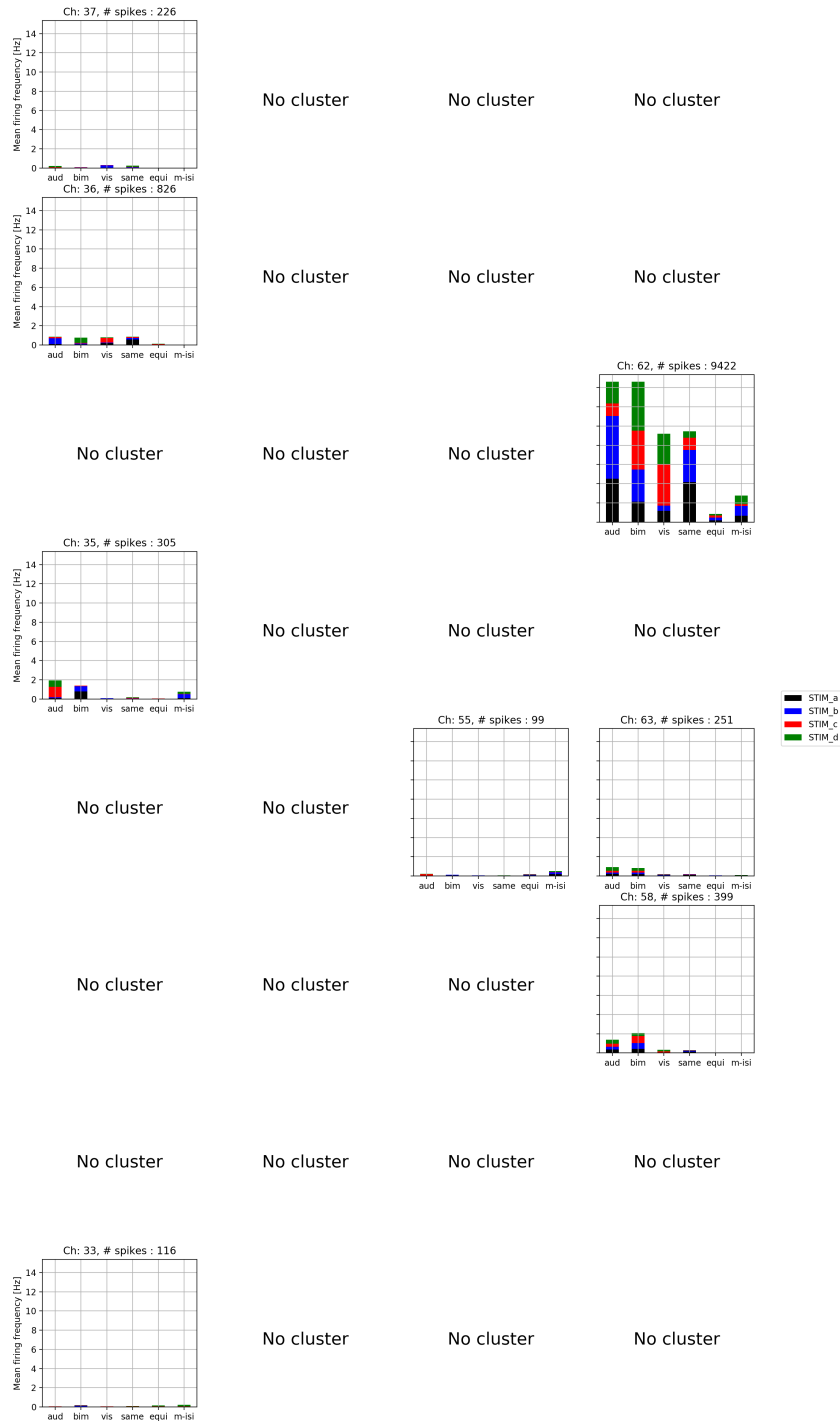


Figure 38. Average firing frequency for the most active cells on each channel at the anterolateral cortex (AL). Bar charts are shown according to real-life placements, channel numbers are ids. Colours are consistently defined by the stimuli (figure 6.). Y-scales are shared across all axis and the total number spikes are noted within the titles.

C Frequency map

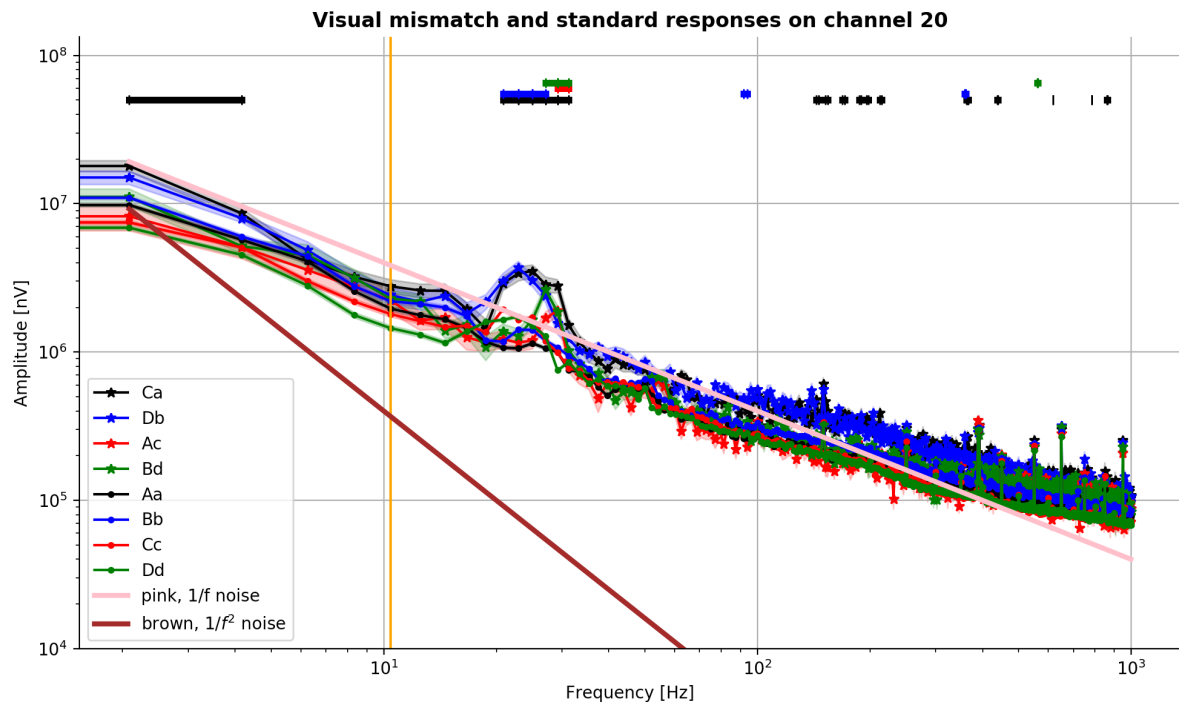


Figure 39. **The presence of pink noise on the data.** Log-log plot of the average Fourier spectra for the traditional visual mismatch and the standards on channel 20. Shaded areas around the lines are the standard deviations. Significant differences are indicated as lines above them and a vertical frequency marker is in orange for reliability. Pink line marks the pink noise ($1/f$ noise) and the brown line is the brown noise ($1/f^2$).

Traditional bimodal mismatch negativity significance map, paired differently

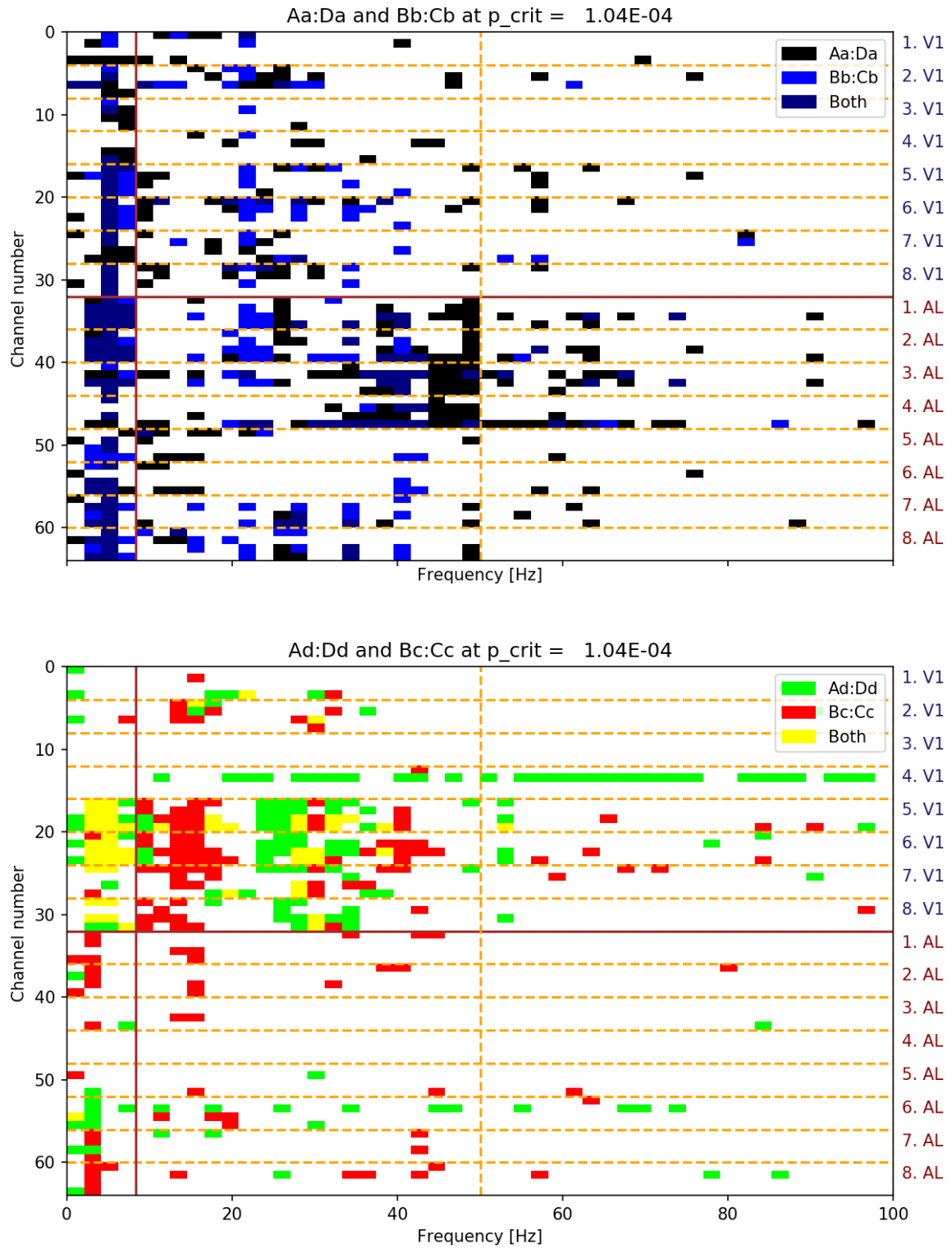


Figure 40. Traditional bimodal mismatch frequency maps paired differently than mentioned in sec. 4.3.5.

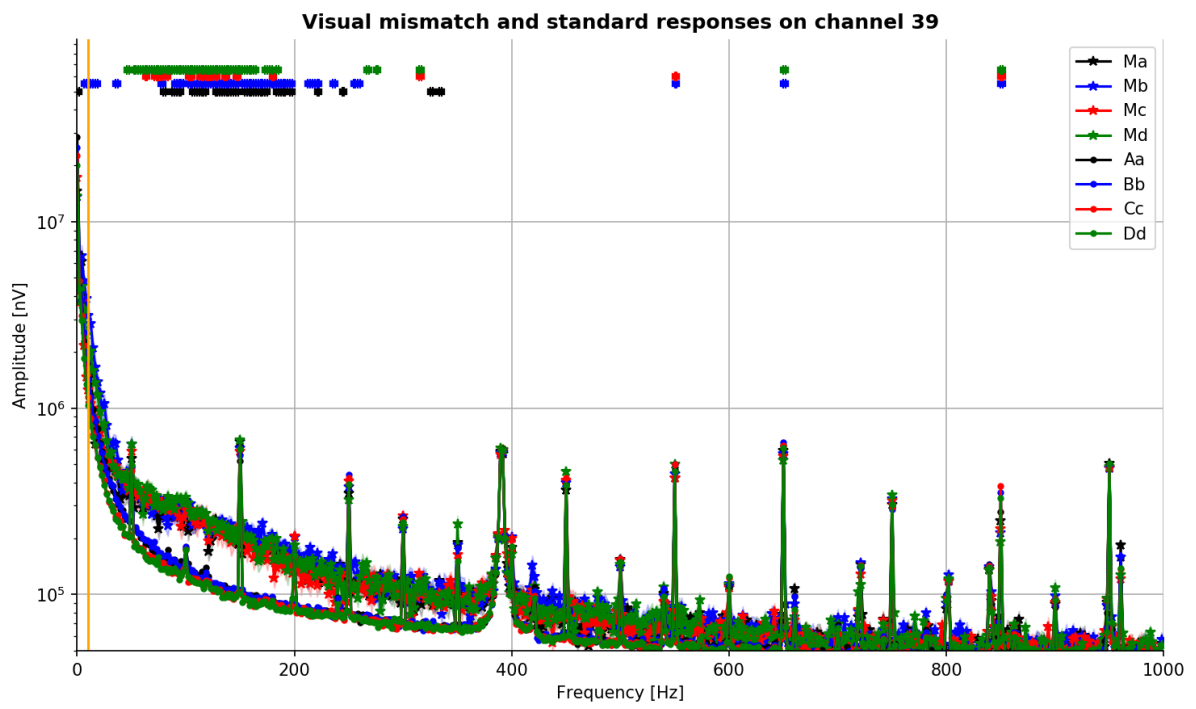


Figure 41. **The Fourier spectra for the standard and M-ISI sequences.** Significant differences marked as lines. Please note that the scale for the frequencies have changed.